Materials Science & Engineering A 827 (2021) 142096

Contents lists available at ScienceDirect

Materials Science & Engineering A

journal homepage: www.elsevier.com/locate/msea

Role of microstructural heterogeneities in damage formation and fracture of oligocrystalline Mg under tensile loading

Evgenii Vasilev, Marko Knezevic *

Department of Mechanical Engineering, University of New Hampshire, Durham, NH, 03824, USA

ARTICLE INFO

Keywords:
Microstructures
Twinning
Dislocations
Fracture
Magnesium

ABSTRACT

This paper describes the main results from *in-situ* and *ex-situ* testing and characterization studies to reveal the effects of microstructural heterogeneities that develop during plastic deformation of coarse-grained Mg on damage formation and fracture of the material. Experiments are carried out using a micro-test tensile stage in and outside a scanning electron microscope in combination with electron backscatter diffraction (EBSD), micro X-ray computed tomography (μXCT), and optical microscopy. It is seen that the micro-specimens exhibit significant macroscopic shape changes upon interrupting the tests. Such shape changes result from microstructural changes and underlying relaxation of inter-granular back-stress accumulated during loading. Twins with low Schmid factor (SF) for basal slip in grains with low SF for basal slip are observed to de-twin. Upon de-twinning, dislocations are found to remain in the structure as is evident by increase in the kernel average misorientation (KAM). Interestingly, twins nucleate in these regions again with continuous forward straining. In contrast, twinned domains favorably oriented for basal slip do not de-twin but thicken with plastic straining. These twins soften the material leading to localization of deformation and damage nucleation. At the interface between twinned domains and parent grains voids are observed. Voids nucleate due to lack of slip transfer causing pile-ups, as is evident from high KAM. Additionally, twins are observed to induce a substantial surface roughness. Large twins accommodating significant shear strain form surface ridges. Such significant heterogeneities also result in nucleation of voids from the surface. In addition to twinning induced voids, damage accumulates and voids form and propagate along high-angle grain boundaries between grains with low SF or those with disparate SF for basal slip. μXCT reveals voids away from the fractured surface highlighting the extent of heterogeneous deformation and fracture behavior of Mg. Fracture surfaces exhibit characteristics of mixed ductile-brittle fracture with signs of *trans*-granular cleavage and fluted facets with minor content of inter-granular fracture.

1. Introduction

Understanding and predicting fracture is fundamental to the design and adoption of improved and new structural materials with enhanced strength, ductility, and toughness. To this end, understanding of the relationship between material structure features and damage nucleation is crucially needed. However, prediction of fracture is a very complex task and progress in this field is impacted by lack of sufficient experimental information. Previous research has shown that microstructural features such as grain, phase, and twin-parent boundaries, inclusions, hydrides, vacancies, and dislocation interaction heterogeneities such as pile-ups can act as initial void nucleation sites [1–8]. Characterization of such microstructural features offers insight into damage nucleation and propagation. As a result, microstructure sensitive models for plasticity and fracture can be developed.

Experiments involving oligocrystalline specimens, i.e. samples containing a small set of coarse grains are often used to study the plasticity-induced heterogeneities because such samples magnify the grain-scale phenomena taking place during deformation [9–14]. Moreover, such specimens are often used to construct models for full-field microstructure evolution simulations [15]. Such studies on pure metals like Al, Ni, Cu, Ta, Ti, and even a steel exist in the literature [9,16–19] but only one on Mg [20]. Thus, this paper is concerned with *in-situ* and *ex-situ* micro-mechanical testing and characterization of pure Mg oligocrystalline specimens to interpret the role of plasticity induced microstructural heterogeneities in damage formation and fracture.

* Corresponding author. University of New Hampshire, Department of Mechanical Engineering, 33 Academic Way, Kingsbury Hall, W119, Durham, NH, 03824, United States.
E-mail address: marko.knezevic@unh.edu (M. Knezevic).

https://doi.org/10.1016/j.msea.2021.142096
Received 26 July 2021; Received in revised form 15 September 2021; Accepted 18 September 2021
Available online 20 September 2021
0921-5093/

1.1. Background on the plasticity of Mg

As understanding of damage and fracture processes is intimately connected and follows plasticity, we briefly review the plasticity of Mg. Deformation mechanisms of Mg alloys at low strain rates have been thoroughly analyzed using conventional *ex-situ* [21–26] and in-situ [27] techniques. Mg and its alloys show poor room-temperature ductility due to a limited number of possible to activate deformation modes. The dominant slip mode is basal <**a**> {0001}, with prismatic <**a**> $\{10\bar{1}0\}$, pyramidal <**a**> $\{10\bar{1}1\}$, first-order pyramidal <**c**+**a**>$\{10\bar{1}1\}$ and second-order pyramidal <**c**+**a**> $\{11\bar{2}2\}$ slip systems also being operative with minor activity [28,29]. Mg also deforms by deformation twinning $\{10\bar{1}1\}$, $\{10\bar{1}2\}$, and $\{10\bar{1}3\}$ depending on crystal orientation relative to the loading direction [21,23,30–35]. Mg exhibits polar behavior [30] as grains undergo or not twinning during compressive versus tensile deformation. Moreover, active mechanisms and related plastic behavior strongly depend on the temperature in addition to the crystallographic orientation relative to an imposed loading direction.

The effect of crystal orientation on deformation behavior is especially pronounced in wrought alloys, which usually exhibit pronounced initial textures. For instance, extension twinning is the dominant deformation mode during the initial stages of deformation in rolled Mg alloy sheets (which have a strong basal-type texture where the **c**-axes of the grains are parallel to the normal direction, ND) when compressive loading is applied in a direction perpendicular to ND. Twinning leads to a reorientation of the lattice for 86° and the **c**-axis of most grains becomes parallel to the applied loading with the maximum shear strain accommodation by twinning of 7.4% [36]. In tension along rolling direction (RD) or transverse direction (TD) of a rolled plate, the Schmid factors (SF) corresponding to basal slip and extension twinning are low and, thus, non-basal slip can activate [21,22]. These differences in the deformation modes as a function of the loading direction lead to an asymmetry in the mechanical response [37,38].

Basal slip is the softest mechanism of plastic deformation in Mg alloys, and it is often accountable for accommodating a significant fraction of the total plastic strain during low-temperature deformation, especially for randomly textured polycrystals, such as cast alloys [23,39]. Although basal slip is the softest mechanism available to Mg, it provides only two independent modes of deformation and is incapable of accommodating strain along the crystallographic **c**-direction. Non-basal slip is much harder than basal <**a**> type and has been considered almost inactive at ambient temperature. However, studies showed that non-basal slip is much more active in Mg and its alloys than previously suspected, based upon single crystal critical resolved shear stresses (CRSS) values [21,40–42]. It was found that non-basal slip can also be responsible for the plastic anisotropy of textured Mg alloy.

Deformation twinning is an important deformation mode in hexagonal close-packed (HCP) metals due to limited amount of easily activated slip systems [43–50]. Twinning depends on chemical composition, crystal lattice orientation relative to the loading direction, and local grain structure [30,51,52]. Activity of deformation twinning increases with increasing grain size [52]. The most commonly observed twinning mechanism, the $\{10\bar{1}2\}$ extension twin provides three additional independent modes, what in combination with two basal slip modes satisfies the Von Mises criterion for uniform plastic deformation. Because the $\{10\bar{1}2\}$ twinning mechanism can only accommodate extension along the **c**-axis, it is activated when crystals are either pulled in tension along their **c**-axes or compressed perpendicular to that direction. Twinning $\{10\bar{1}2\}$ is known to be responsible for the tension–compression asymmetry that is normally observed in textured Mg alloys and causes lower yield stress, enhanced hardening and ductility. In contrast, compression along **c**-axis is the least ductile and leads to formation of $\{10\bar{1}1\}$ twins.

Some $\{10\bar{1}2\}$ twins are seen when the applied stress resolves onto the twin planes in the 'wrong' sense [53]. One rationalization for these observations is that $\{10\bar{1}2\}$ twins form following unloading in response to the localized stress redistribution within the structure. The redistribution of stresses during unloading might be expected to give rise to stresses, in certain grains, opposite to those imposed during deformation.

The other commonly observed twining mode is $\{10\bar{1}1\}$ twinning associated with contraction of **c**-axis. Important role of this type of twinning is reorientation of crystal lattice in "soft" directions, favorably oriented for basal slip, especially in double twinning $\{10\bar{1}1\} - \{10\bar{1}2\}$ [54,55]. This preferential alignment of basal planes in the interiors of these twins can lead, in single crystals, to softening, rapid unloading, high strains, void formation and ductile failure [56,57].

Twins nucleate in regions of stress concentrations [52,58,59] such as grain boundaries [59,60] and dislocation structures. Twin nucleation is favored at low angle boundaries, which are also favorable for the transfer of twins over them [61]. Nucleation may require high local stresses and may be followed by very rapid growth to a certain size. Twin nucleation occurs under stresses considerably greater than those required for twin growth [62,63].

With the introduction of a twin there is a considerable redistribution of local stresses. These can be considered as 'forward' stresses at the twin tip, and 'back' stresses in the twin interior and adjacent surrounding regions [55,61,64]. As the twin thickens, these back stresses build up to the point where thickening halts [65]. That helps to explain why de-twinning is so common in Mg. The process of $\{10\bar{1}2\}$ de-twinning occurs under stresses lower from those required for twinning during deformation in the opposite direction. CRSS for $\{10\bar{1}2\}$ twin growth is also lower than that for twin nucleation because $\{10\bar{1}2\}$ twinning dislocations are very mobile due to their wide core width, the reason for extension twins to easily grow in size until they reorient nearly the whole grain. In contrast, $\{10\bar{1}1\}$ contraction twins are thin. These twins usually form multiple thin lamellae. Contraction twins form an internal extension twin, which is the commonly observed "double twin" sequence. The internal extension twin inhibits thickening of this double twin by loss of twin/matrix coherency [66].

Twinning is also autocatalytic, in the sense that twin formation stimulates further twin nucleation and a cascade of twinning spreads over a volume. Twinning events in one grain stimulate twinning events in neighboring grains and thereby, in strongly textured samples, twinning controls the flow stress [67]. As the twin frequency rises, the perturbation of the local stress states is likely to increase which can give rise to Lüders-like twin cascades. It may also generate 'anomalous' twins on planes and in grains where they might not be otherwise expected. With higher twin frequencies, subsequent twinning events will relate more to the local perturbed stress and less to the applied stress. Conversely, one might therefore expect twins that form initially to be more sensitive to the applied stress and to the SF. Although twins may form in consequence of the local stress state, they will only adopt an appreciable thickness if favored by the applied stress. That is, twin thickening will obey a CRSS law.

Although widespread values of the CRSSs have been reported for the various slip and twinning systems in pure Mg and alloys, it is established that the CRSS follows the trend CRSS basal $<$ CRSS extension twinning $<$ CRSS prismatic $\leqslant$ CRSS pyramidal at room temperature with typical CRSS non-basal/CRSS basal ratios ranging between 20 and 100. The ratio of CRSS values of basal slip to extension twinning in single crystals falls in the range of 1: 2–4 [68].

The CRSS for basal slip and $\{10\bar{1}2\}$ twinning are believed to be approximately temperature and strain-rate independent [39]. However, the CRSSs of prismatic and pyramidal systems decrease as the temperature increases [39,51,69,70]. Thus, the activity of these non-basal slip systems increases with temperature. It also should be noted that even though CRSS values from well-prepared single crystals have fundamental significance, they do not directly reflect the applied shear stresses that are necessary to activate different slip modes in polycrystalline materials [71]. For correlation of grain orientation with

activity of slip and twinning, SF and slip trace analysis have been widely used [72–75]. However, there are multiple evidences that $\{10\bar{1}2\}$ twins do not always obey this law due to local stress gradients within a grain and the stochastic nature of twin nucleation [76–78].

In many studies on Mg and Mg alloys [54–57,79–83], twinning and especially double-twinning has been correlated to flow localization in the vicinity of its boundaries followed by void formation. This correlation has been associated with substantial crystal reorientations within the twinned regions and underlining shifts in slip activity due to the change in mechanical fields. The twinned region of a contraction twin is typically much more favorably oriented for easy basal slip than the original parent crystal [84]. The intense basal slip activity that results within the thin lamella region of the double twin produces a localized shear that cannot be accommodated across the twin interface and ultimately leads to void formation. The change in local mechanical fields may cause formation of additional twins as well as influence secondary twinning, de-twinning, and existing twin expansion rates [85–88].

1.2. Objectives

In this paper, *in-situ* and *ex-situ* tensile tests and characterization are carried out on micro-tensile samples of coarse-grained Mg to study plasticity induced heterogeneities, damage, and fracture. The characterization combines electron backscattering diffraction (EBSD) performed in a scanning electron microscope (SEM) in conjunction with SF, kernel average misorientation (KAM), and slip trace analyses. Furthermore, scanning electron microscopy of fracture surfaces (fractography), micro X-ray computed tomography (μXCT) imaging of voids, and optical microscopy are also performed. We examine microstructural features including twins, slip traces, voids, and microcracks occurring during tensile loading and unloading of coarse-grained pure Mg. Observations and findings across multiple scales from macroscopic shape changes of tested samples originated from back-stress fields and microstructure to evolution of microstructural heterogeneities induced by deformation twinning and slip to damage and fracture are presented and discussed in this paper.

2. Material and experimental procedures

Mg of purity 99.98% (Table 1) rolled in a 10 mm thick plate was used in this study. In order to grow grains and create oligocrystalline Mg, the rolled material was annealed in argon atmosphere at 450 °C for ~24 h to grow very large grains. The annealed material was cut into 2 mm thin plates by spark erosion and milled into tensile specimens (see Appendix, Figure A1).

Specimen preparation included mechanical grinding on abrasive paper up to 2500 grit and subsequent chemical polishing in 10% solution of HNO_3 in ethanol up to mirror finish.

Mechanical testing was performed using a Gatan microstage with max load of 2 kN. Tension was performed both *in-situ* and *ex-situ* along RD of rolled sheet with elongation increments of ~0.05 strain. For *in-situ* samples, loading was stopped and SEM/EBSD imaging performed. For *ex-situ* samples, surface imaging was done after unloading and removing sample from the tensile machine. Tescan Lyra SEM with EDAX EBSD system was used for imaging and EBSD mapping at 16–20 kV. Scan were taken such that the entire gauge section of the sample was covered and then panoramas were stitched from multiple images. Step size was selected so every map contains from 500,000 to 1,000,000 points. EBSD data procession was performed in TSL OIM 8.0, including cleanups: grain confidence index (CI) standardization, neighbor CI correlation, and discard of data with CI less than 0.1.

Optical microscopy was performed on a confocal laser scanning microscope Olympus OLS-5000 using ×10 objective MPLFLN10XLEXT. The images were taken using violet laser in high dynamic range (HDR) mode and stitched into panoramas.

X-ray computer tomography (μXCT) was performed on a Zeiss Xradia 610 Versa tomography under applied voltage and power at the tube of 40 kV and 1W respectively. 4× objective was used with source and detector distanced by 17 mm from the sample which resulted in the voxel size ~1.5 μm. Scans were performed in 1601 projections per 360° and then reconstructed into 3D tomogram with drift correction in Dragonfly software. In the analysis, more than 7 connected empty voxel were highlighted as internal voids.

Slip trace analysis [89–91] was used to identify the active slip systems from the secondary electron (SE) SEM images and the EBSD orientation data input using a MATLAB code [92]. Slip trace analysis included detection of slip traces on the secondary electron images. Possible slip traces and SF for a given orientation of a crystal and applied loading were calculated from the cross product of the slip plane normal (in the sample coordinate direction) with the specimen Z direction [75]. Five slip modes were considered in the analysis:

$\{0001\}\langle\bar{1}\bar{1}20\rangle$: basal $\langle a\rangle$
$\{\bar{1}100\}\langle\bar{1}\bar{1}20\rangle$: prismatic $\langle a\rangle$
$\{\bar{1}101\}\langle\bar{1}\bar{1}20\rangle$: pyramidal $\langle a\rangle$
$\{10\bar{1}1\}\langle11\bar{2}3\rangle$: first-order pyramidal $\langle c+a\rangle$
$\{\bar{1}\bar{1}22\}\langle11\bar{2}3\rangle$: second-order pyramidal $\langle c+a\rangle$

Calculated traces were compared to experimental observations and active slip mode was determined.

3. Results

Considering the ratio between sample size and grain size, the initial microstructure varies from sample to sample (Fig. 1). Typically, only a few large grains are present in the gauge section per specimen predominantly orientated with their **c**-axis nearly perpendicular to the tension direction. In *sample #2* a set of smaller grains was obtained. Due to the very limited number of grains per cross-section, texture characterization is not performed. In some cases, a single grain occupied the whole cross section. Twins identified as tensile $\{10\bar{1}2\}$ were also observed in the initial microstructure. These twins result from sample preparation and tightening.

Fig. 1a–e show inverse pole figure (IPF) maps of the initial microstructure and stress-strain response per tested sample. *Samples #1* and *#2* were tested *in-situ*. The experimental *in-situ* setup required long working distance 18–20 mm from the electron gun to the sample surface decreasing the quality of diffraction, especially on deformed samples. To improve the quality, the rest of the samples were tested *ex-situ*. Moreover, the *ex-situ* tests went to larger strains. Coarse-grained structures lead to highly heterogeneous mechanical response of the material. As is evident, *in-situ* samples failed earlier than *ex-situ*. The latter samples last longer likely due to relaxation upon the test interruption, which will be elaborated shortly. While some samples exhibit relatively uniform elongation and hardening (Fig. 1b'-c'), some fracture even after relatively low strain (Fig. 1a'). While the samples yield at approximately 10 MPa, hardening rates are substantially different as a consequence of deformation mechanisms i.e. dislocation slip and twinning. Similarity in their yield stress suggests that plasticity starts by slip, while the hardening slope is different whether the deformation proceeds by more slip

Table 1
Content of impurities in pure Mg.

Element	Al	Ca	Cd	Cu	Fe	Mn	Ni	Pb	Si	Sn	Zn
Content, ppm	37	10	<1	10	32	29	6	<2	10	<10	10

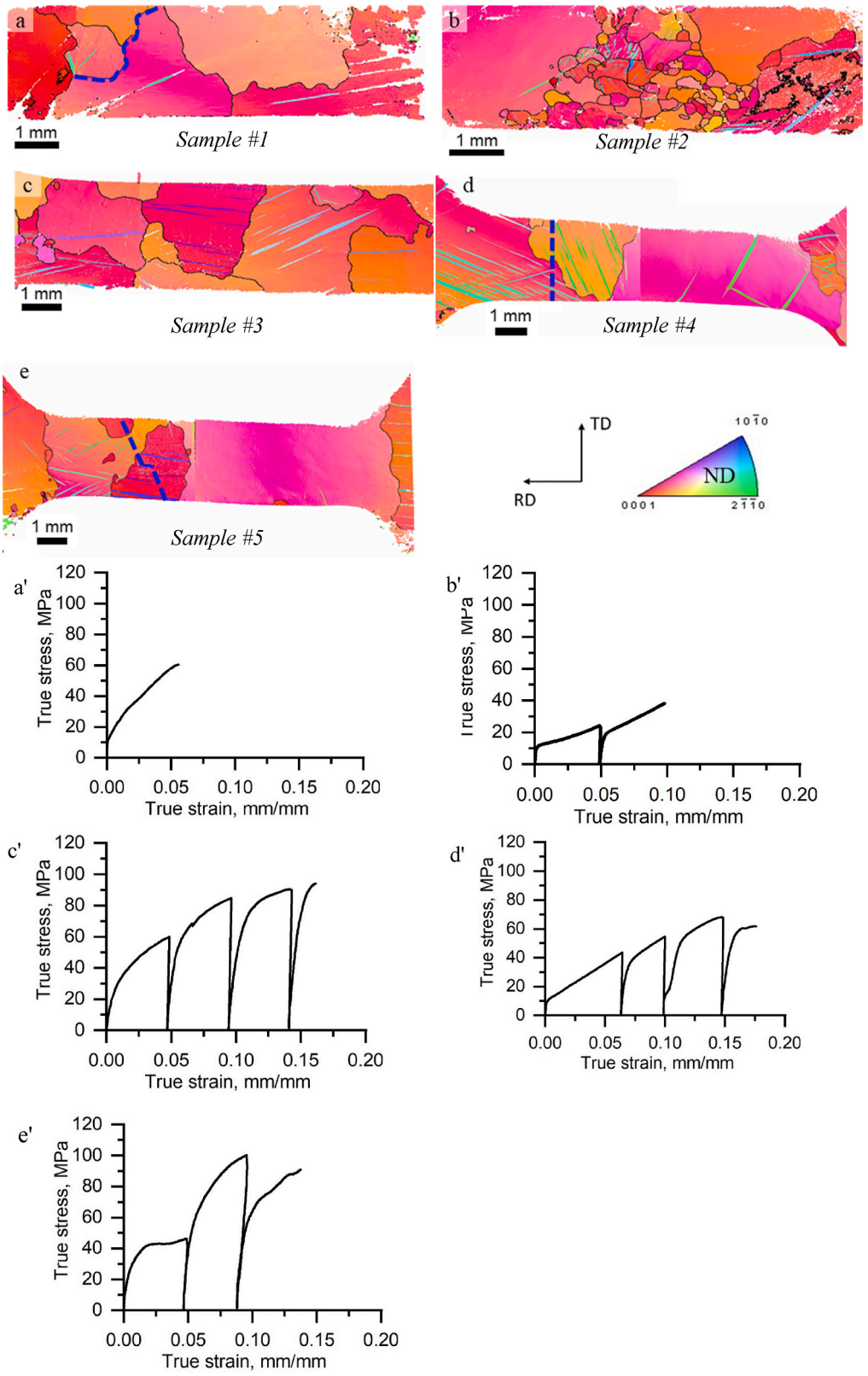

Fig. 1. (a–e) IPF maps showing the initial microstructure in the coarse-grained micro tensile specimens of pure Mg. (a'-e') corresponding true stress-true strain curves upon testing of the specimens from (a–e). Specimens in (a–e) are numbered in the text as *sample 1–5* for referencing. *Samples 1* and *2* are deformed *in-situ*, while *samples 3–5* are deformed *ex-situ*. The sample direction perpendicular to the maps is ND as indicated in the standard IPF triangle. The colors in the IPF maps represent the orientation of ND sample axis with respect to the crystal lattice frame according to the coloring in the standard IPF triangle. Blue dash lines indicate the locations of some partial or the final fracture i.e. separation mapped to the initial microstructural state. The locations of final fracture for samples in a, b, and c are out of view and will be shown in Fig. 11 and Figure A4. (For interpretation of the references to color in this figure legend, the reader is referred to the Web version of this article.)

(causing high hardening rate) or more twinning (causing low hardening rate). For example, Fig. 1a' and c' stress-strain curve show a hardening typical for predominance of slip, while Fig. 1b' and e' shows signs of predominance of twinning reflected in low hardening rate.

3.1. Macroscopic shape changes upon unloading

Ex-situ deformed *samples 3–5* exhibit substantial macroscopic distortion (Fig. 2). As will be shown later, grains neighboring the distortion/bending regions possess high SF values for basal slip and exhibit high strain localizations. The shape changes are a consequence of relaxation of inter-granular back-stress fields originating primarily from geometrically necessary dislocations (GNDs), which were built up during forward loading. In single-phase polycrystalline metals back-stresses develop from interactions between individual grains of different crystal orientation during deformation. The origin of these back-stresses is the anisotropy of grains with different crystal orientation, which causes varying properties over a material volume. These inter-granular stresses are known as the type II stresses [93–101]. A harder grain surrounded by softer grains will undergo lower plastic deformation than its surrounding neighbors. Incompatibility of accommodated plastic strain between the grains causes accumulation of dislocations around the strong grain, which results in the plastic strain gradient. Microstructural changes during uniaxial tension of coarse-grained Mg are substantial not only as a consequence of crystallographic slip but also due to deformation twinning. Twins significantly alter local stress states [102,103]. Moreover, tensile $\{10\bar{1}2\}$ twins in Mg are very large and often have distorted shape, which is a consequence of high local inhomogeneity in microstructure and mechanical fields. The behavior of twinning and de-twinning also governs the relaxation in part upon unloading and strain reversal. The local microstructure plays an important role in twin activation and de-twinning, besides the dependence on crystallographic orientation and grain size [72,104–107]. These slip/twinning phenomena are significantly enhanced with the size effect intrinsic to the studied oligocrystalline samples relative to conventional polycrystalline Mg alloys, in which such macroscopic shape changes upon unloading are not appreciable. As a result, the distortions are significant.

3.2. De-twinning and fields of kernel average misorientation

The processes of twinning and de-twinning within a single grain are depicted on Fig. 3 for a sample tested *ex-situ*. Evidently, after 0.05 strain, existing twins shrink and almost completely disappear (de-twinning). After 0.1 strain more twins appear in the same area and de-twin after loading to 0.15 true strain.

CRSS for de-twinning is smaller than that for nucleation of a new twin as well as back-stress aids de-twinning and thus it can easily operate. Another explanation can be in bending of the sample and grain rotation with respect to the loading direction. In this case, stress state within a grain becomes different from uniaxial tension and non-Schmid behavior of twinning is observed, especially when combined with unloading.

Upon de-twinning and underlying plastic relaxation, dislocations are left in the structure and value of kernel average orientation is increased. After loading to 0.1 strain, twins nucleate again in the same area due to presence of existing dislocations and KAM increases even further. And finally, after straining to 0.15 existing twins de-twin and disappear again and higher KAM is observed in the area of de-twinning.

3.3. Schmid factor (SF) analyses

SF was calculated for basal slip with respect to the loading direction. Fig. 4a and b show *sample 4* in the initial state and after loading to 0.15 strain. On the macroscopic scale, ROI 2 exhibits significant distortion. The key difference noted on the SF maps in Fig. 4a and b is that the ROI 2 has a high SF for basal slip while it is much lower in the ROI 1. This leads to intensive basal slip in ROI 2. The detailed view of ROI 2 is shown on Fig. 4c and d with two key grains 2 and 3. While grains #2 and #3 in the area have similar SF for basal slip, twins within these grains have very low and very high basal slip SF, respectfully. In grain #2, "hard" twins act as barriers for dislocation motion while "soft" twins in grain #3 stimulate basal slip and potentially transmission of the slip into the parent grain intensifying the plastic deformation in grain #3 [108]. Note that 'hard' and 'soft' refer to basal slip activity. In contrast to ROI2, twinning and de-twinning operate in ROI 1. Interestingly, twins with high SF for basal slip do not de-twin (ROI 3 and 4 on Fig. 4e and f), while those twins surrounding the ROI 3 and 4 do de-twin. The twins that de-twin have low SF for basal slip. In summary, twins with low SF for basal slip in grains hard for basal slip de-twin upon unloading, while twins with high SF for basal slip in grains hard for basal slip and any twins in grains soft for basal slip do not de-twin but grow in number and thickness with plastic strain. It is expected that during unloading of the sample, grains experience a substantial change in their stress state due to inter-granular back-stress fields and even compressive stress followed by plastic recovery during which twins with low SF for basal slip easily de-twin, while those with high SF likely experience reverse dislocations glide.

Another example of "soft" twins formation within a grain hard for basal slip is shown in Fig. 5. After loading to 0.05 and 0.1 strain, formation of twins is observed near the grain boundary between grains #4 and #5. These twins rapidly increase in numbers and area upon straining. Meanwhile, the rest of the grain #5 remains free of twins (Fig. 5e). SF map (Fig. 5d) shows that the newly formed twins in grain #5 have very soft orientation for basal slip. Such softening promotes formation of new twins with soft orientations, which leads to damage development and rapid localization of deformation. Increase in the number of twins is the autocatalytic nature of twinning. Once started, twins cause local stress redistribution, dislocations generation, and promotion of new twins formation in the same and adjacent grains, especially in regions of high back-stresses such as neighborhood of existing twins. This explains why twins form predominantly in the localized area of grain #5 and not in the rest of the grain. Note that grain #4 is also developing twins soft for basal slip.

3.4. Deformation twinning induced surface roughness and voids

In very coarse grains, lateral dimensions of twins are large with twin length reaching 1 mm and more. These gigantic twins are observed to

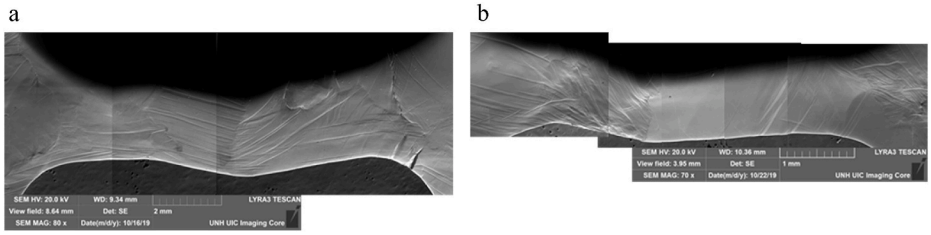

Fig. 2. SEM images showing extent of the macroscopic distortion during *ex-situ* loading of: (a) *sample 3* at a strain of 0.1 and (b) *sample 4* at a strain of 0.1.

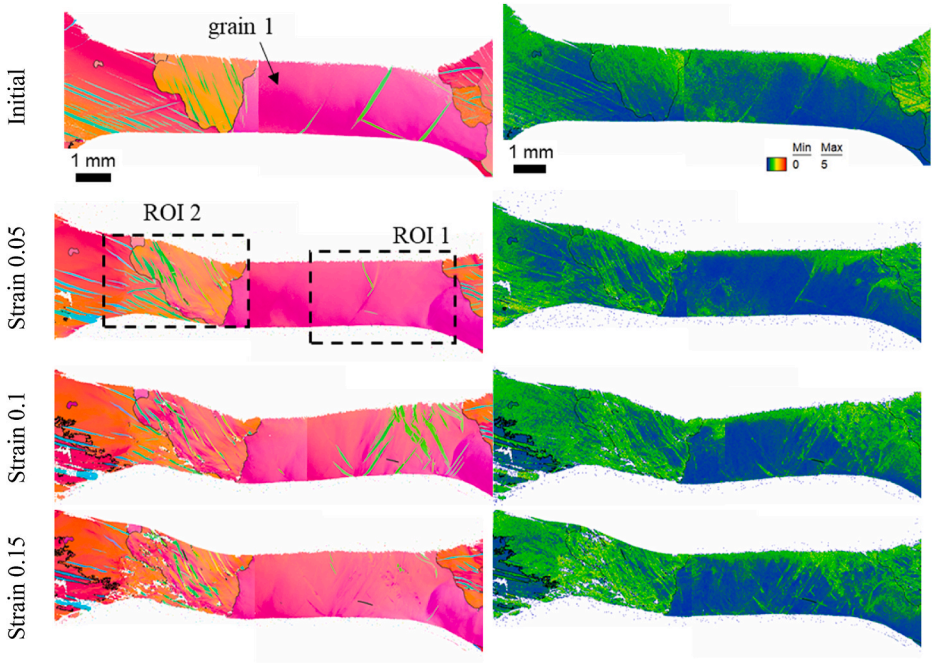

Fig. 3. Evolution of grain structure depicted using IPF maps (images in the left column) and KAM maps (images in the right column) as a function of strain during simple tension for the coarse-grained pure Mg *sample 4*. Regions of interest (ROI) are indicated by the black dash line. Note that the KAM scale bar provided in this figure applies to all KAM maps in this paper.

produce significant shear strain on the surface resulting in formation of ridges. Fig. 6 highlights typical morphological characteristics of twins. Twins often have sharp lenticular morphology and distorted shape (Fig. 6a) resulted from highly heterogeneous deformation. Twins produce significant shear strain on the surface resulting in formation of ridges and geometrical incompatibilities (Fig. 6b), especially at twin-twin and twin-grain intersections. This creates high local inhomogeneity in microstructure and mechanical fields and can lead to void nucleation on the free surface of the sample (Fig. 6c), including twin-grain boundary (Fig. 6d and e) if twin transmission through the grain boundary is not favorable like in Fig. 6a. With sharp lenticular shape twins can also act as stress concentrators at their tips (Fig. 6f).

3.5. Formation of voids

Fig. 7 shows another example of heterogeneity development and nucleation of voids associated with twinning. As described earlier, there are multiple twins with soft orientation for basal slip in grain 3 of *sample 4* at a strain of 0.1. A few voids are observed at the twin-grain boundary interface. The KAM map shows no significant variance in the local misorientation. After straining to 0.15, twins grow developing higher local misorientations, as shown in the KAM map. With soft orientation of twins and also relatively soft orientation of the parent grain for basal slip, dislocation likely transfer though the twin boundary initially and after an intense amount of slip pile-up and form voids.

Another major observation of damage development and voids in pure coarse-grained Mg is attributed to boundaries between grains with low SF for basal slip. As seen in Fig. 8 and confirmed by multiple similar observations on this and other samples, grain boundary cracking predominantly happens between such grains with low SF for basal slip. This observation is the most frequent one among all observed voids in all samples, suggesting its importance in damage nucleation. Corresponding KAM maps show lack of plasticity within all such regions. In the absence of twinning, hard orientations for basal slip lack sufficient deformation mechanisms for strain accommodation and fail at the weakest link, which is the grain boundary.

Fig. 9 shows another example of cracking at grain boundaries between grains having disparate SF for basal slip. It has been reported that the ductility of Mg alloys is influenced by grain boundary cracking [91], which is dependent on grain boundary misorientation and underlying grain boundary cohesion. The figure shows a crack propagating along high-angle grain boundaries, consistent with previous studies [1, 91,109]. For a high-angle grain boundary, slip systems on each side of the grain boundary are generally not coplanar. Consequently, the high-angle grain boundaries act as barriers to gliding dislocations, with the dislocations piling up at grain boundaries. Coalescence of a number of dislocations can open cracks in grain boundaries. Considering that the *sample 1* did not fracture at the location shown in the figure indicates that heterogeneities due to twinning and intense slip carrying out the plasticity at other locations contribute more to the ultimate fracture than these grain boundary cracks.

3.6. Fractography of fractured surfaces

Fractured surfaces of pure Mg consist of smooth *trans*-granular planes and *trans*-granular fluted facets with a minor content of dimples. Fig. 9 depicts regions for each of these features. Low roughness of smooth faces allows observation of slip lines occurring mostly on a single plane. Moreover, the smooth areas exhibit morphology of deformation twins either a level lower than the surrounding smooth surface (pulled out from the surface) or a level higher than the surrounding smooth area (pulled out from the other surface). In contrast, rough surface of flutes makes it nearly impossible to distinguish slip lines or twins. The smooth *trans*-granular planes likely run through the grains of limited plasticity accommodation, while the rough surfaces are through the grains of pronounced plasticity accommodation. Fig. 10f depicts ductile dimples as a consequence of micro-void coalescence. Location of the final fracture for these two samples and *sample 5* is shown in Fig. 11. As is evident, the final fracture is *trans*-granular.

μXCT (Fig. 12, video in the supplementary material of the paper) gives additional insight into structure of a fractured sample. Clusters of internal voids having spherical/elliptical and tubular-shape as well as secondary cracks can be observed. In particular, the figure shows voids adjacent to the fracture surfaces as well as those in the vicinity of

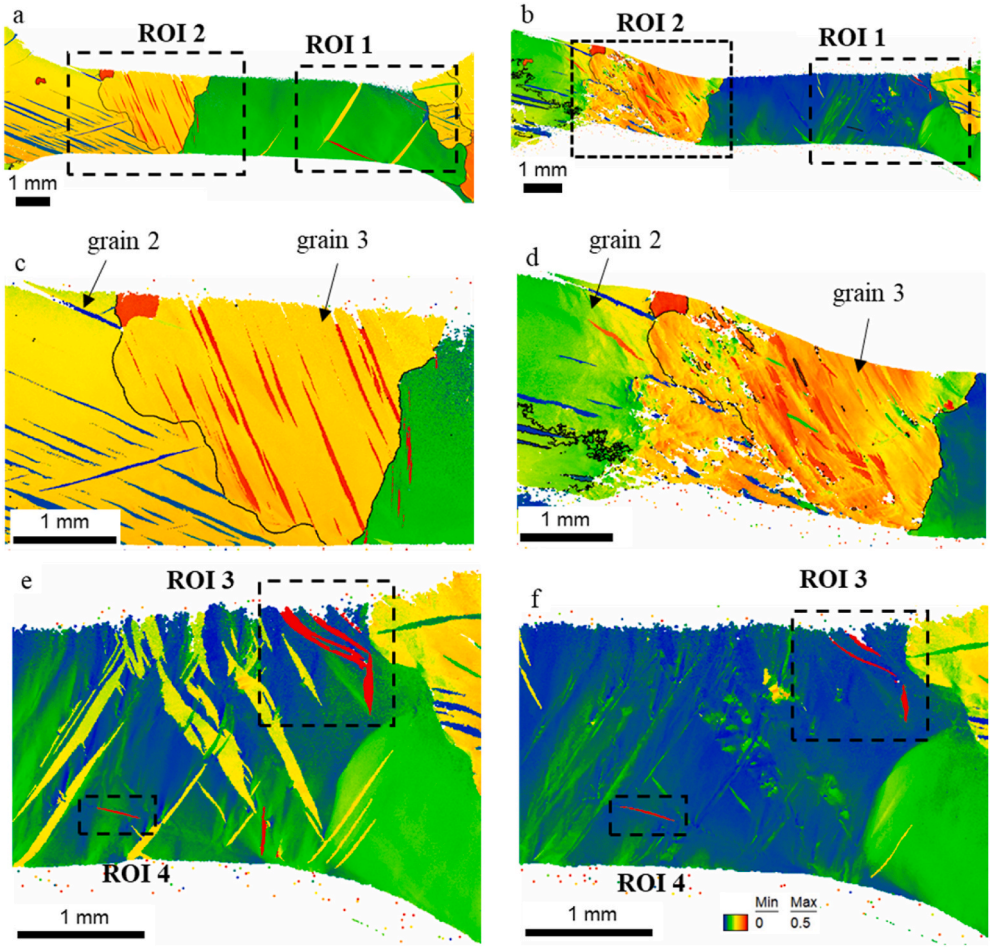

Fig. 4. SF maps for basal slip relative to the loading direction for *sample 4*: (a, c) the initial sample state and (b, d) after 0.15 strain. (c and d) are magnified ROI 2. (e, f) are magnified ROI 1, after 0.1 and 0.15 strain, respectively. Twins with high SF for basal slip are noted in ROI 3 and 4. Note that SF scale bar presented in this figure applies to all SF maps in this paper.

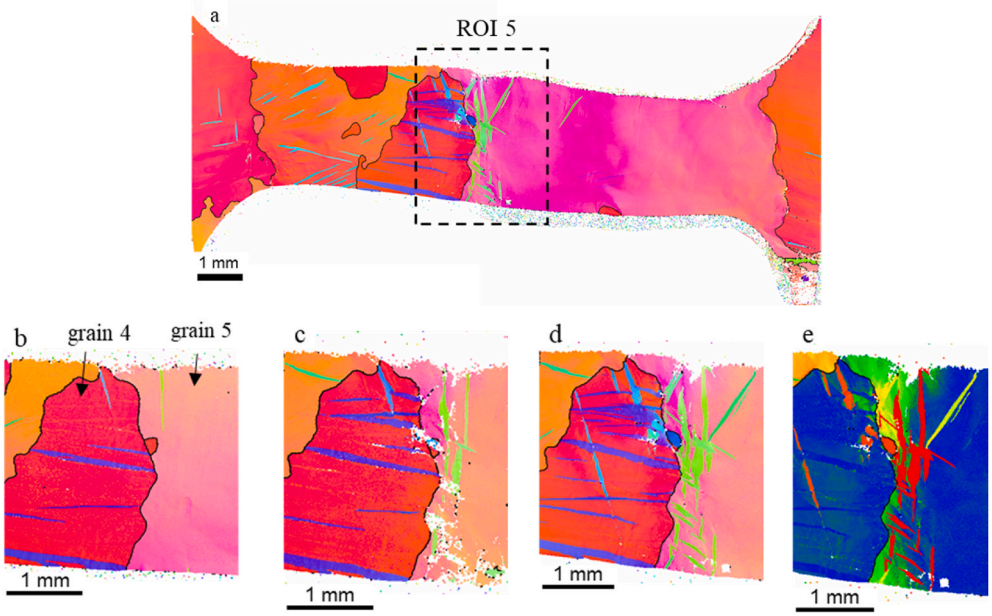

Fig. 5. Evolution of microstructure during straining of *sample 5*: a – overview of the sample at a strain of 0.1. (b–e) are magnified ROI 5 showing (b–d) IPF maps at 0, 0.05, and 0.1 strains, respectfully, and (e) SF map for basal slip at a strain of 0.1.

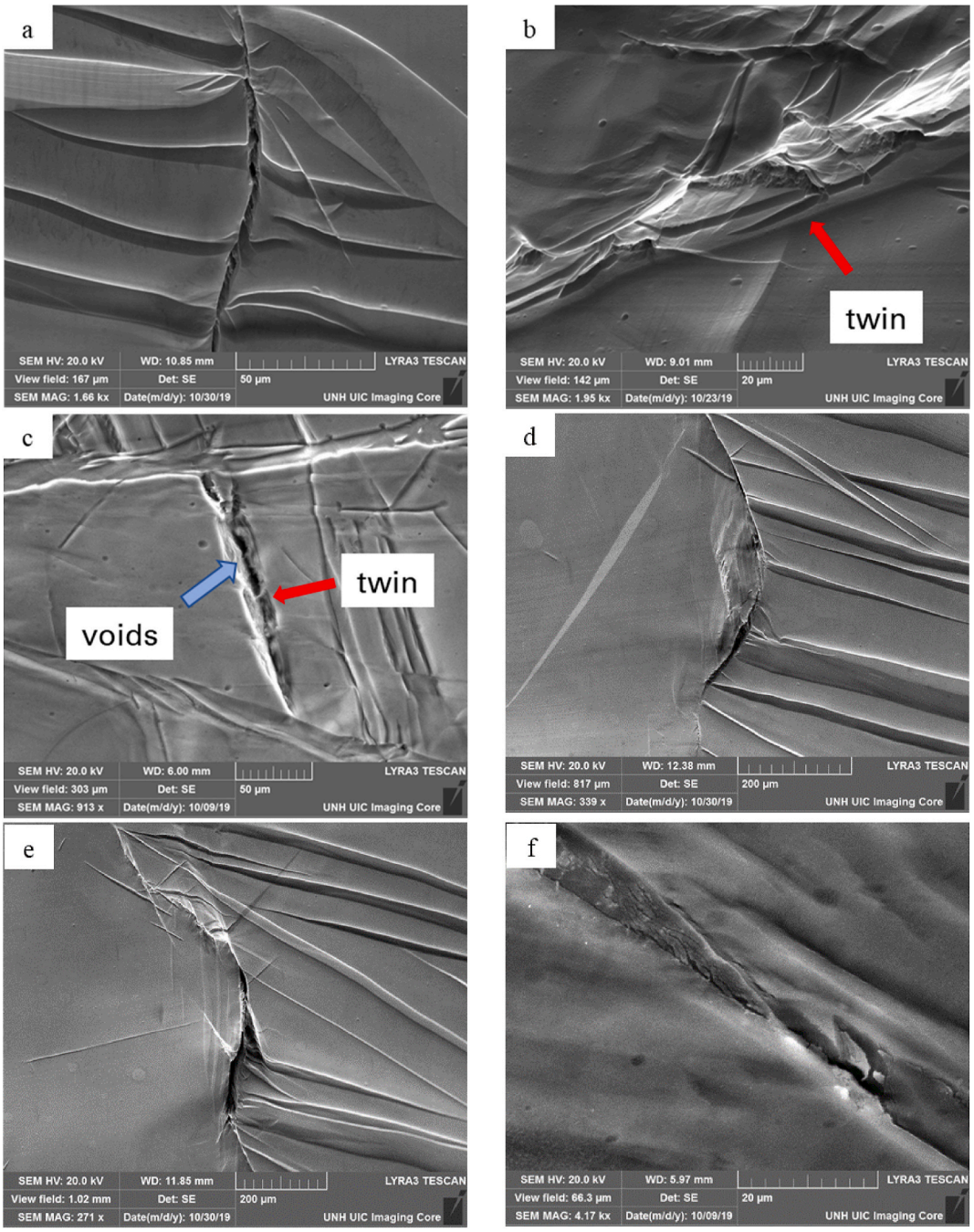

Fig. 6. Morphological features of twins: (a) distorted shape, (b) surface ridge, (c) surface ridges resulting in void nucleation, (d, e) formation of voids at twins impeding grain boundaries, (f) crack at a twin tip. (c, f) – *sample 1* at a strain of 0.05, (b) – *sample 3* at a strain of 0.15, (a, d, e) – *sample 4* at a strain of 0.1.

secondary cracks.

Tubular-shaped voids and their clusters can have two origins: twins [57] or intersections of slip planes [110]. Tubular voids formed by twins are usually longer and single-standing, while those slip-based are shorter and tend to form clusters. This comes from observations that twins forming tubular voids are discrete and large in size, while intersections of basal and non-basal slip planes forming tubular voids are small and numerous.

4. Discussion

Ductile fracture in tension is frequently associated with some form of strain localization and usually includes localized necking. The localization is slowed down by the hardening of the material with increasing strain. Conversely, localization can be accelerated when there is a loss in hardening rate or, more dramatically, if softening occurs. Strain induced softening, for instance, can arise from a number of microscopic factors such as predominant deformation in a single grain favorably oriented for basal slip or in a twined domain reoriented for easy basal slip.

4.1. Mechanical behavior and corresponding microstructural changes with an emphases on role of twinning

The observed microstructural changes are used to discuss the plasticity and fracture behavior of the material. In the first loading of *sample 5* (Fig. 1e), hardening rate is low which is associated with active twinning and growth not causing substantial hardening. The microstructural observations in Fig. 5 show that twinning is reorienting grains for easy

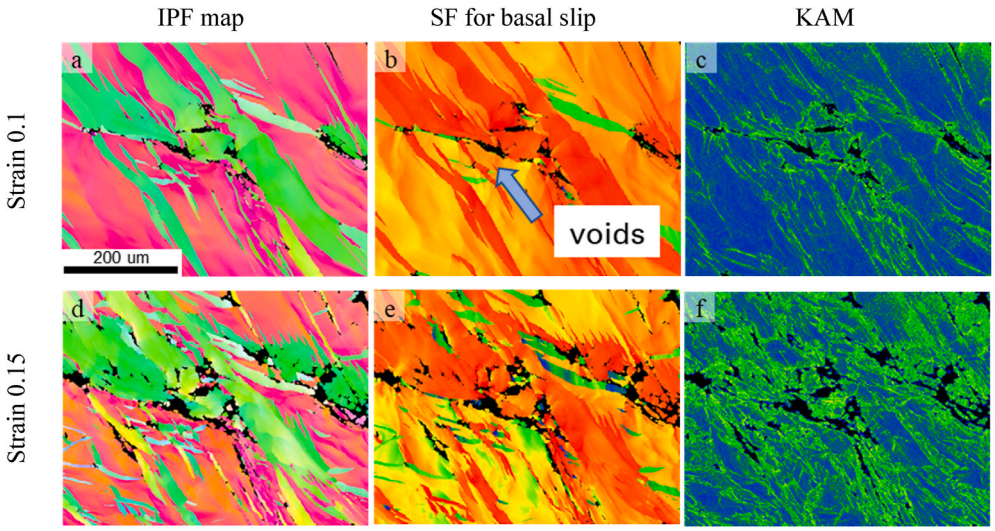

Fig. 7. Twin-induced formation of heterogeneities and voids in *sample 4*. Location of the area on the sample is shown in Figure A2 of the appendix. The 200 μm micronbar applies to all images.

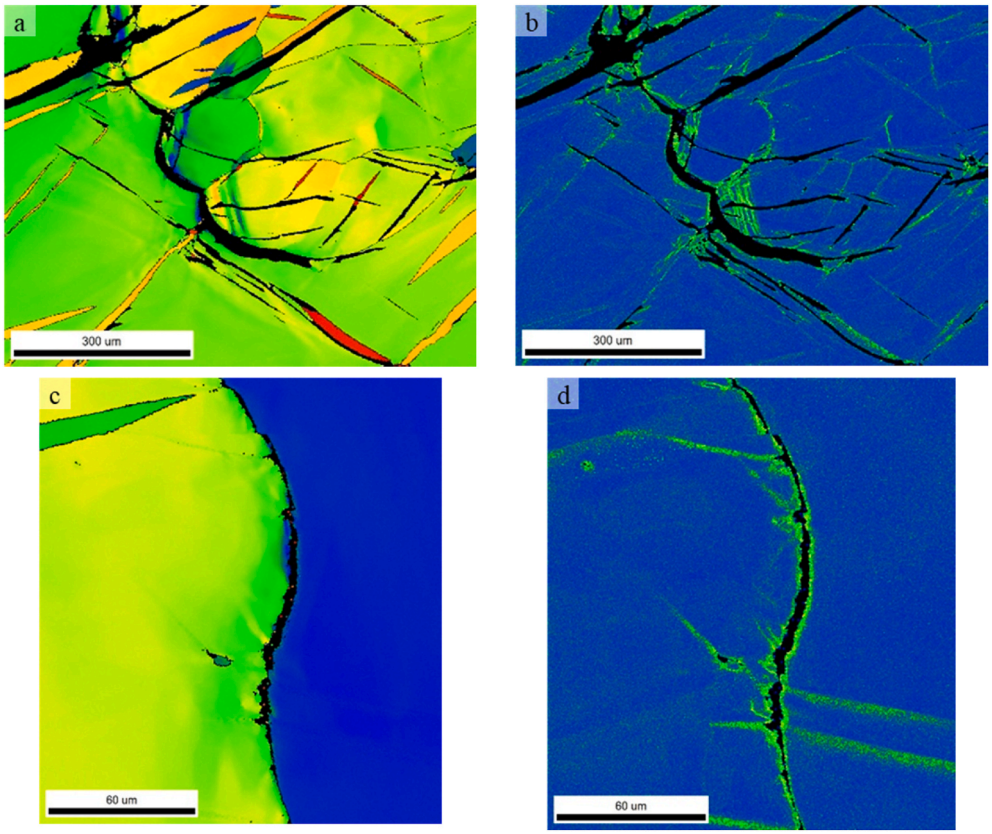

Fig. 8. Formation of voids at grain boundaries between grains with low SF for basal slip: (a, b) – *sample 2* at 0.1 strain, (c, d) – *sample 3* at 0.05 strain. (a, c) – SF maps for basal slip, (b, d) – KAM maps. These areas on the samples are shown in Figures A3 and A4 of the appendix.

slip. In the second loading of the same sample, significant hardening is observed and attributed to hardening of basal slip in the soft twinned domains and neighborhood regions. Finally, in the third loading up to 0.15 strain, instabilities develop due to twinning induced damage localization and the sample fracture *trans*-granularly.

The stress-strain curve of *sample 4* exhibits a linear increase in hardening (Fig. 1d'), which is attributed to the activity of both deformation twinning and dislocation slip. Localizations are observed in the regions easy for basal slip in both parent grains and twins. In such regions twins could be transparent to dislocation glide in the early stage of deformation before crystallographic reorientations [111]. The reorientations due to active slip in the twinned domains increase SF for basal slip relative to the pulling direction, while the neighboring grains are relatively intensive. The region of intense slip becomes site of damage nucleation and eventual *trans*-granular fracture. The observed twinning-de-twinning regions in the *sample 4* occurring due to the *ex-situ* methodology of testing did not influence the localization.

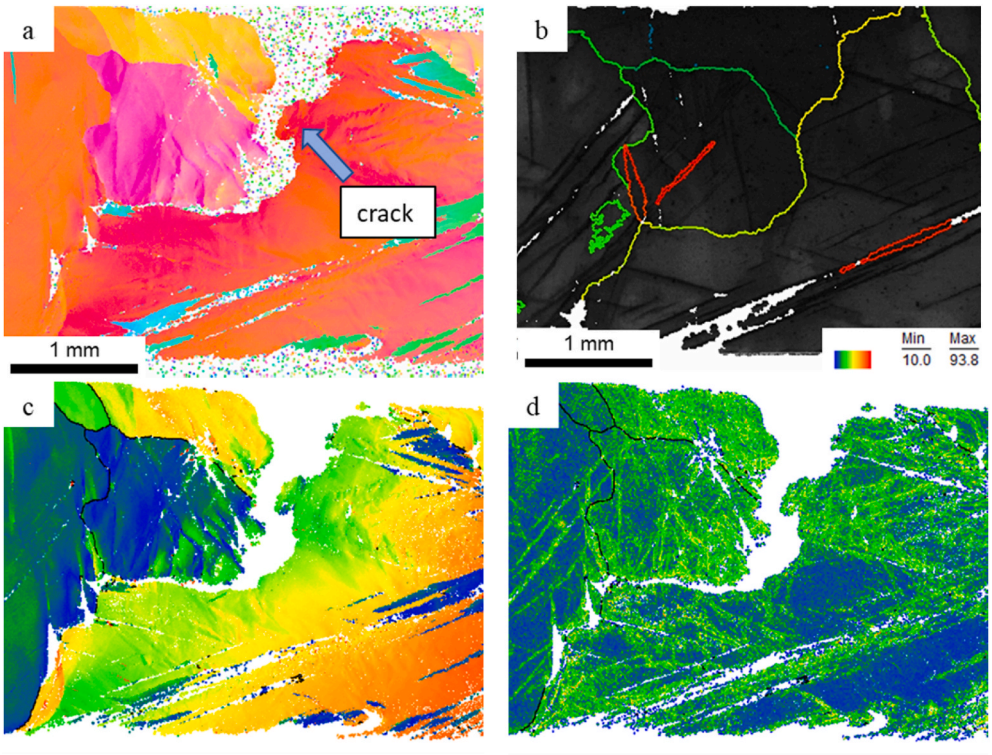

Fig. 9. (a) An IPF map of a region of *sample 1* showing de-cohesion at grain boundaries after 0.05 true strain, (b) a grain boundary map for the region in its initial state, (c) SF map for basal slip, (d) – KAM map. This area on the sample is shown in Figure A5 of the appendix.

4.2. Mechanical behavior and corresponding microstructural changes with an emphases on role of slip

In order to determine active slip mode in grains adjacent to observed voids, slip trace analysis was performed. Slip traces were observed but not in all grains. There are several reasons for no slip traces being observed in some grains. For example, it is possible that dislocations did not move to the sample surface or the amount of dislocations was not large enough, or slip could not be resolved in the SEM. In addition, slip traces would not be expected to be observed when Burgers vectors are parallel to the surface being observed. In most cases, only one set of slip traces was observed for one grain. In rare cases, traces of two slip systems were identified in one grain. Although it is possible that multiple slip systems could have been activated in a single grain, traces for three or more slip systems were never identified.

In most of the grains and twins, adjacent to microvoids, basal slip traces are found to be the dominant ones. Even in cases with low SF for basal slip, basal slip is dominant due to the extremely low CRSS compared to non-basal modes. However, we do not neglect the possibility of activation of non-basal modes at the later stage of deformation, but their role in damage nucleation is likely low. The presence of fluted morphology in fracture surfaces suggest the activity of non-basal slip modes during fracture as intersections of basal and non-basal slip planes are believed to be onset of tubular voids.

The role of basal slip is not only to carry out the plasticity in the soft regions but also the formation of dislocations pile-ups at impenetrable boundaries leading to formation of voids as shown in Fig. 13 at multiple twin-grain boundaries and triple junctions. The effect is especially pronounced at boundaries between grains or twins with disparate SF for basal slip.

Basal slip and tensile twinning, being the easiest modes of deformation in pure Mg, provide 5 independent systems to satisfy the von-Mises criterion. When one or both of these mechanisms is hard to be realized due to texture [28], non-basal slip or contraction twinning mechanisms could activate. However, their activation is very difficult due to much higher CRSS, especially in pure and coarse-grained material as in the present work. Limited basal slip and extension twinning due to crystal orientations in the samples being parallel with ND and difficulties to activate non-basal slip and contraction twinning can lead to void formation and crack propagation along grain boundaries. Although formation of voids at grain boundaries and de-cohesion between grains with high SF or with one having a low value of SF for basal slip were observed, the path of ultimate fracture for the samples was not in between the grains.

4.3. Mechanical behavior and corresponding microstructural changes with an emphases on voids and fractography

The results of the present study show that fluted and smooth facets are the most common fracture morphologies observed after tension to fracture of pure Mg. Fluted facets are associated with plastic deformation in the close-to-the-crack region. The fluted fracture surface markings are well-known in HCP metals such as titanium [112], zirconium [113,114] and Mg [110,115]. In these studies it was concluded that fluted fracture surfaces are produced by the coalescence of tubular voids nucleated at regions of high strain along the line of intersection of slip bands (or intersection of slip bands with grain boundaries) ahead of crack tips. For Mg, fluted fracture surfaces parallel to $\{10\bar{1}X\}$ planes are produced because tubular voids are nucleated by the intersection of basal slip bands with prismatic or pyramidal slip bands. Micro-voids can subsequently form in highly strained regions between tubular voids producing more equiaxed dimples [110]. We observed multiple voids of tubular shape by μXCT. Besides these, spherical/elliptical micro-voids are also identified, especially near micro-cracks confirming the development of ductile fracture in pure Mg. In addition, reliefs of twin boundaries over the smooth brittle regions indicate the presence of intensive plastic deformation within twins oriented for easy basal slip and subsequent pile-ups at their boundaries forming voids.

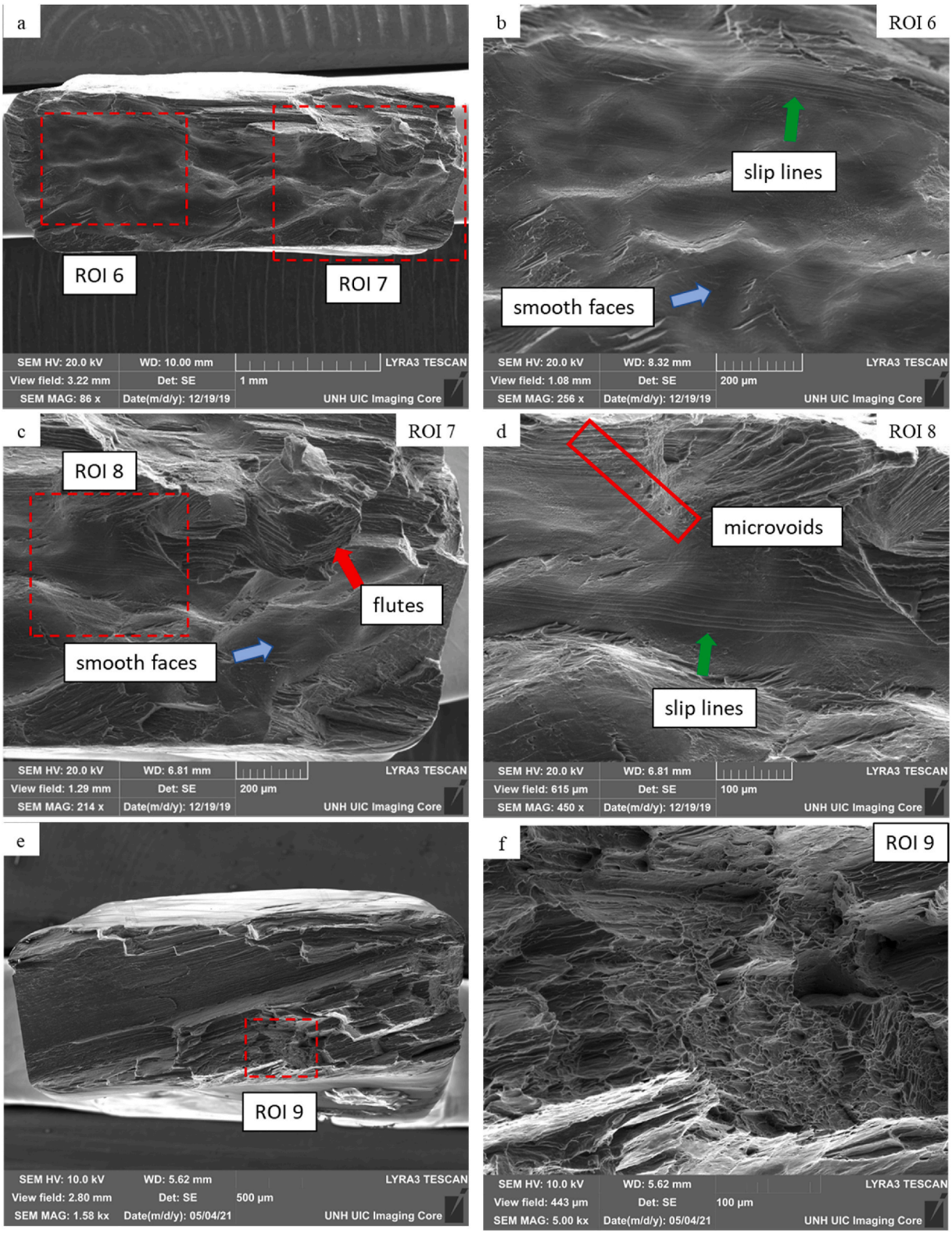

Fig. 10. SEM images of fractured surfaces: (a) the entire fracture surface of *sample 1*, (b) magnified ROI 6, (c) magnified ROI 7, (d) magnified ROI 8, (e) the entire fracture surface of *sample 2*, (f) magnified ROI 9.

5. Conclusions

In this work, we have presented a novel set of experimental data on plasticity of oligocrystalline Mg. The data includes a number of direct observations into the effects of microstructural heterogeneities that develop during plastic deformation of pure Mg with weak rolling texture on damage formation and fracture under tensile loading. The heterogeneities leading to damage nucleation, voids, and fracture are a consequence of spatially non-uniform activity of twinning and slip-interface interactions. The development of high heterogeneity of the

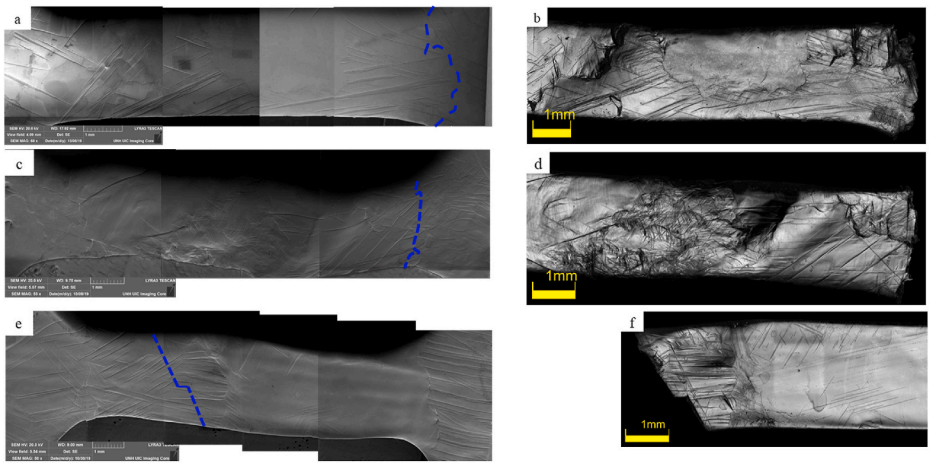

Fig. 11. SEM images (a, c, e) and corresponding optical images showing fractured halves (b, d, f) of: *sample 1*, (a) undeformed, (b) fractured half; *sample 2*, (c) at 0.1 strain, (d) fractured half; *sample 5*, (e) at 0.1 strain, and (f) fractured half. The blue dashed lines indicate the final fracture. (For interpretation of the references to color in this figure legend, the reader is referred to the Web version of this article.)

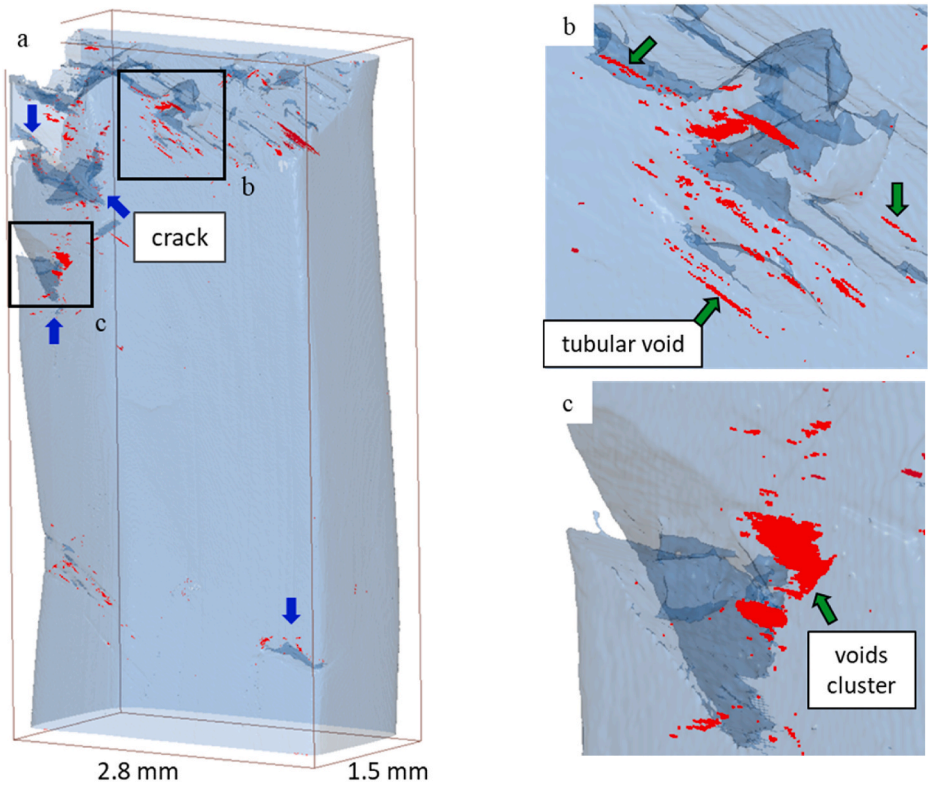

Fig. 12. μXCT of fractured *sample 3*: (a) overview of the sample with (b) magnified view of the region indicated in (a) highlighting tubular voids, (c) magnified view of region indicated in (a) highlighting voids cluster. Light blue color represents surface mesh, which is semi-transparent; whenever there is an overlap of semi-transparent surfaces, light blue color changes to darker blue; voids are highlighted by opaque red color. Secondary cracks are indicated by blue arrows. (For interpretation of the references to color in this figure legend, the reader is referred to the Web version of this article.)

plastic deformation is initially evident from the macroscopic distortion of tested samples, which is attributed primarily to relaxation of inter-granular back-stresses accumulated during loading in *ex-situ* testing. The relaxation is the reason for *ex-situ* tested specimens to stretch more than *in-situ* tested specimens. The back stresses fields are also a reason for the observed de-twinning of twins with low SF for basal slip in grains hard for basal slip. The developed dislocation structure at the sites of disappeared twins causes repeated appearance of twins upon continuous forward straining.

The primary reason for nucleation of voids are twinned domains, which are easy for basal slip. Strain incompatibilities and lack of slip transfer between adjacent twin and grain boundaries causes pile-ups growing into voids. Moreover, lack of independent slip systems sufficient to accommodate an applied deformation near high angle grain boundaries between hard grains or those with disparate SF for basal slip also opens voids. Finally, twins are found to create high surface roughness and structure heterogeneities, which promote void formation from the surface. With sharp lenticular shape, surface twins can act as stress concentrators. Interplay of these factors leads to fracture.

A combination of limited plasticity accommodation in hard and pronounced plasticity accommodation in soft grains/twins results in mixed ductile-brittle appearance of fractures surfaces with signs of *trans*-granular cleavage and fluted faces. Multiple tubular voids and clusters of micro-voids as well as secondary cracks are observed near and away from the fractured surfaces highlighting the extent of heterogeneous deformation and fracture behavior of Mg. Coalescence of tubular-type

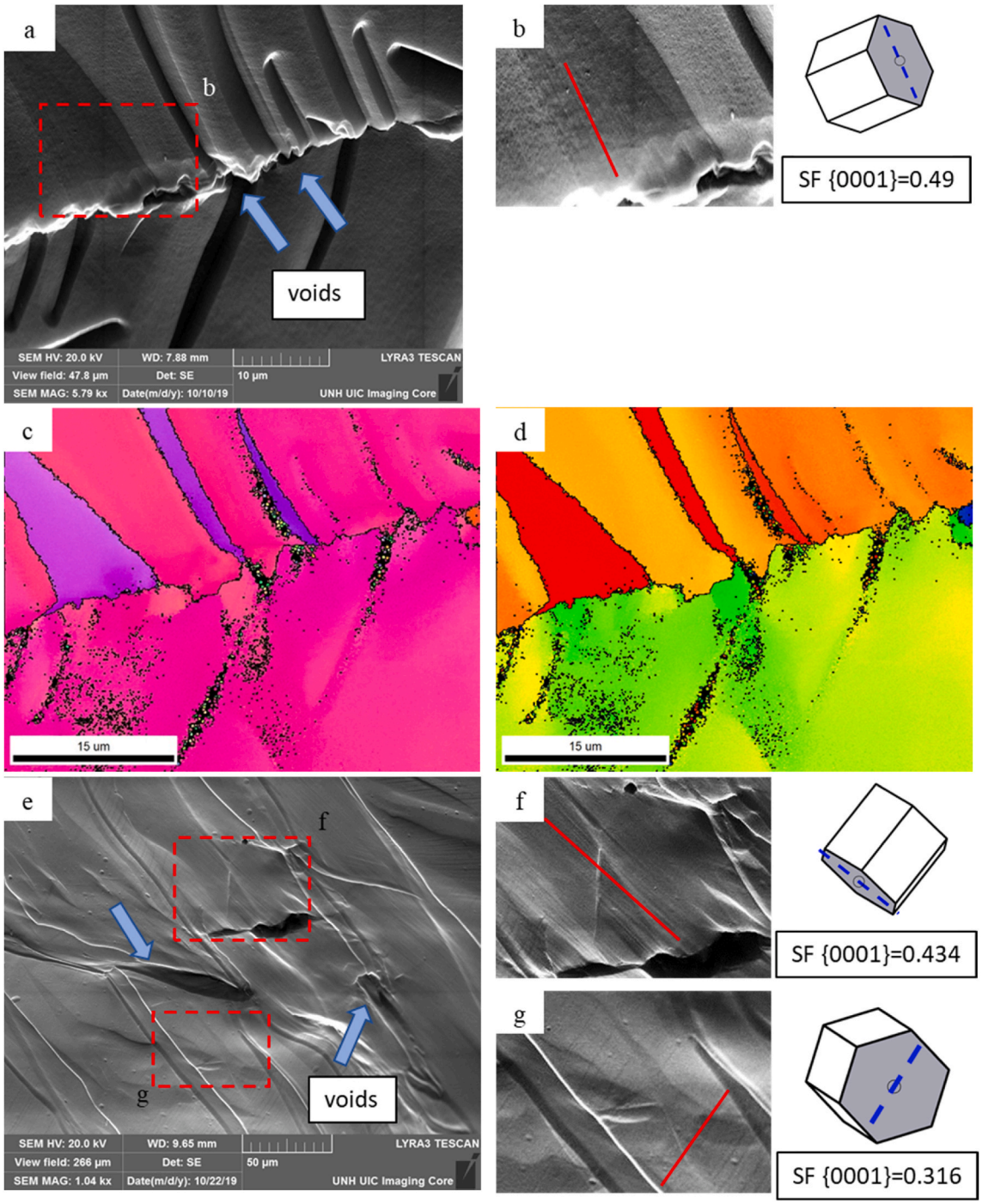

Fig. 13. Slip trace analysis: (a–d) *sample 2* at 0.1 strain*:* (a) SEM image, (b) magnified area from (a) showing slip traces, (c) IPF map, (d) SF map for basal slip; (e–g) *sample 4* at 0.1 strain: (e) SEM image, (f, g) magnified areas from (e) showing slip traces (IPF and SF maps are provided in Fig. 7). The identified slip traces on the SEM image are indicated by the red solid lines, while the calculated slip traces are the blue dashed lines in the hexagons. Blue arrows point to voids. Location of the depicted areas on the samples are shown in Figures A6 and A2, respectively of the appendix. (For interpretation of the references to color in this figure legend, the reader is referred to the Web version of this article.)

voids forms fluted fracture surfaces, while micro-voids form a minor content of dimples. Although voids at grain boundaries and de-cohesion between grains occur, these do not play a major role in the final fracture.

CRediT authorship contribution statement

Evgenii Vasilev: Methodology, Validation, Formal analysis, Investigation, Data curation, Writing – original draft, Visualization. **Marko Knezevic:** Conceptualization, Methodology, Investigation, Resources, Writing – review & editing, Supervision, Project administration, Funding acquisition.

Declaration of competing interest

The authors declare that they have no known competing financial interests or personal relationships that could have appeared to influence the work reported in this paper.

Acknowledgements

This research was sponsored by the U.S. National Science Foundation and was accomplished under the CAREER grant no. CMMI-1650641. The authors acknowledge Professor Thomas R. Bieler of Michigan State University for providing the code for slip trace analysis and discussions related to the analysis.

Appendix

Fig. A1 shows the test specimen geometry. Fig. A2, Fig. A3, Fig. A4, Fig. A5, and Fig. A6 depict locations for several regions of interest (ROI).

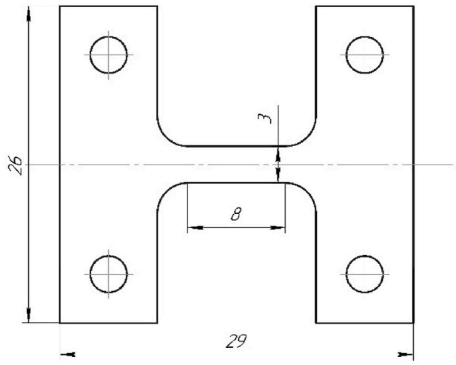

Fig. A1. Geometry of a micro-tensile sample. Thickness is 2 mm.

Fig. A2. Location of ROI depicted in Fig. 7 (*sample 4* at a strain of 0.1). Note that the straight dividing lines sometime occurring in the maps are an artifact of stitching of separate IPFs taken with some detector distortion commonly occurring at low magnification.

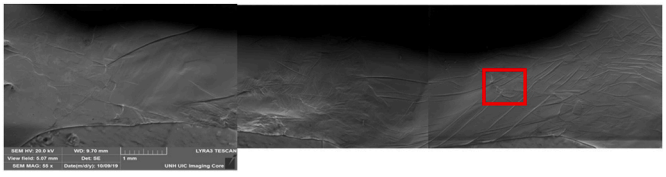

Fig. A3. Location of ROI depicted in Fig. 8a and b (*sample 2* at a strain of 0.1).

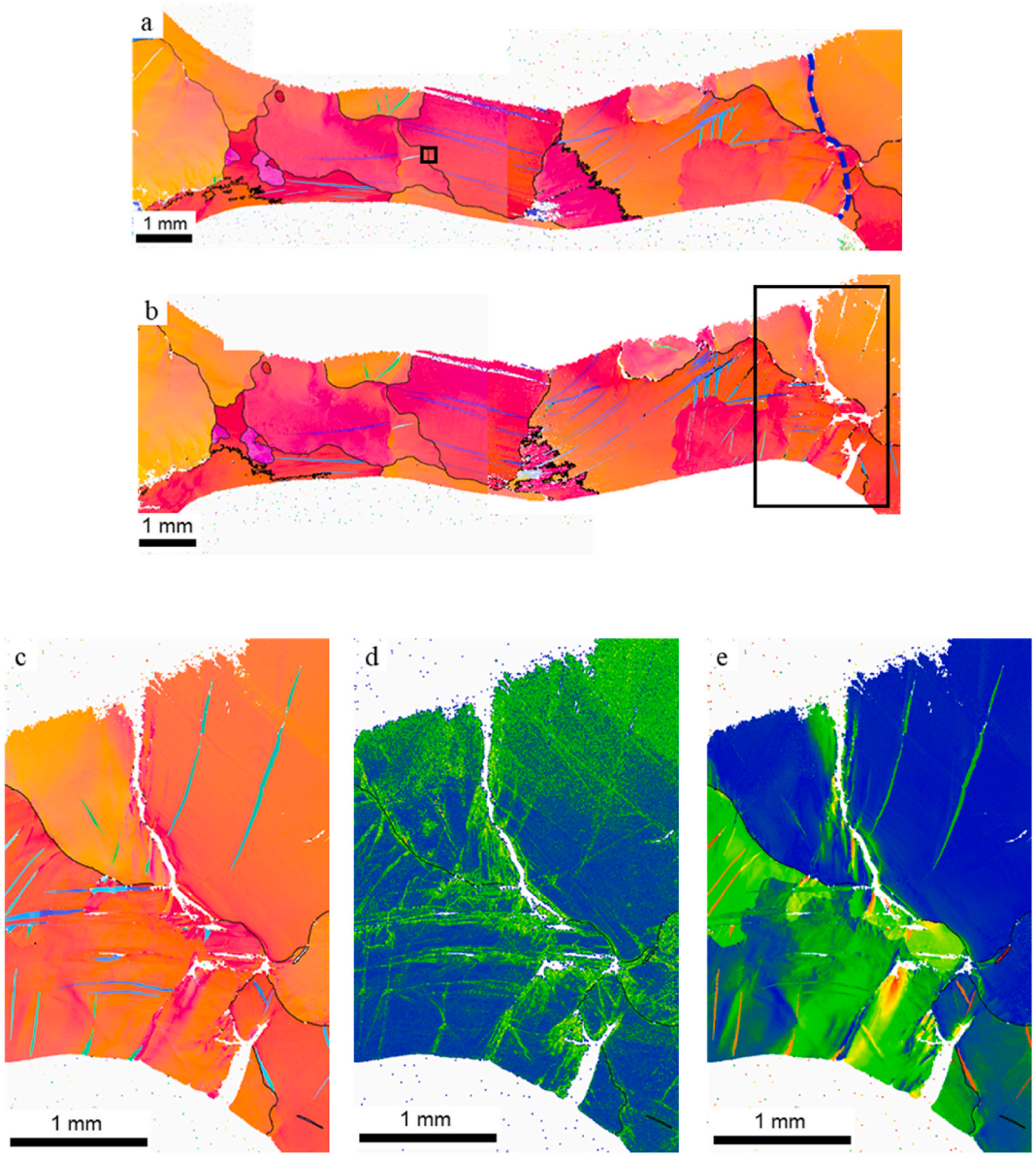

Fig. A4. (a) Location of ROI depicted on Fig. 8 c and d. *Sample 3:* (a) at 0.1 strain, (b) at 0.15 strain. (c-e) magnified area from (b) showing another example of cracks at grain boundaries between grains with low SF for basal slip: (c) IPF map, (d) KAM map, and (e) SF map. The blue dashed line indicates the final fracture.

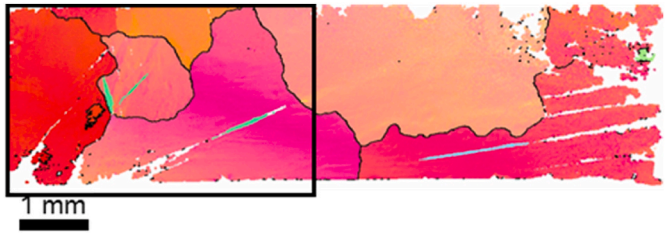

Fig. A5. Location of ROI depicted on Fig. 9 (*sample 1* in its undeformed state).

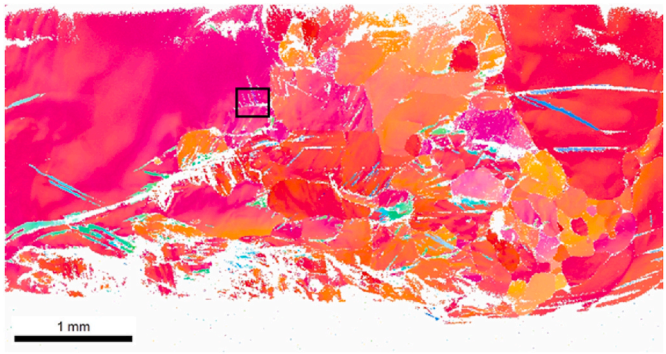

Fig. A6. Location of ROI depicted on Fig. 13a–d (*sample 2* at a strain of 0.1).

Data availability

The raw/processed data required to reproduce these findings cannot be shared at this time due to technical or time limitations.

References

[1] J. Shi, M.A. Zikry, "Grain–boundary interactions and orientation effects on crack behavior in polycrystalline aggregates, Int. J. Solid Struct. 46 (21) (2009) 3914–3925.

[2] W.M. Ashmawi, M.A. Zikry, Grain boundary effects and void porosity evolution, Mech. Mater. 35 (3) (2003) 537–552.

[3] Y. Zhang, P.C. Millett, M. Tonks, B. Biner, Deformation-twin-induced grain boundary failure, Scripta Mater. 66 (2) (2012) 117–120.

[4] T. Dümmer, J.C. Lasalvia, G. Ravichandran, M.A. Meyers, Effect of strain rate on plastic flow and failure in polycrystalline tungsten, Acta Mater. 46 (17) (1998) 6267–6290.

[5] T. Al-Samman, G. Gottstein, Room temperature formability of a magnesium AZ31 alloy: examining the role of texture on the deformation mechanisms, Mater. Sci. Eng., A 488 (1–2) (2008) 406–414 [Online]. Available: http://www.sciencedirect.com/science/article/B6TXD-4R7NR6G-2/2/b37137b55e26205d2d3cf115afe79416.

[6] J. Kadkhodapour, A. Butz, S. Ziaei Rad, Mechanisms of void formation during tensile testing in a commercial, dual-phase steel, Acta Mater. 59 (7) (2011) 2575–2588, https://doi.org/10.1016/j.actamat.2010.12.039.

[7] J. Wang, et al., Origins of high ductility exhibited by an extruded magnesium alloy Mg-1.8Zn-0.2Ca: experiments and crystal plasticity modeling, J. Mater. Sci. Technol. 84 (2021) 27–42, https://doi.org/10.1016/j.jmst.2020.12.047.

[8] K.J. Tam, M.W. Vaughan, L. Shen, M. Knezevic, I. Karaman, G. Proust, Modelling the temperature and texture effects on the deformation mechanisms of magnesium alloy AZ31, Int. J. Mech. Sci. 182 (2020), 105727, https://doi.org/10.1016/j.ijmecsci.2020.105727.

[9] Z. Zhao, M. Ramesh, D. Raabe, A.M. Cuitiño, R. Radovitzky, Investigation of three-dimensional aspects of grain-scale plastic surface deformation of an aluminum oligocrystal, Int. J. Plast. 24 (12) (2008) 2278–2297, https://doi.org/10.1016/j.ijplas.2008.01.002.

[10] E. Demir, I. Gutierrez-Urrutia, Investigation of strain hardening near grain boundaries of an aluminum oligocrystal: experiments and crystal based finite element method, Int. J. Plast. (2021), https://doi.org/10.1016/j.ijplas.2020.102898.

[11] D. Raabe, M. Sachtleber, H. Weiland, G. Scheele, Z. Zhao, Grain-scale micromechanics of polycrystal surfaces during plastic straining, Acta Mater. 51 (6) (2003) 1539–1560, https://doi.org/10.1016/s1359-6454(02)00557-8.

[12] N. Zhang, W. Tong, An experimental study on grain deformation and interactions in an Al-0. 5%Mg multicrystal, Int. J. Plast. (2004), https://doi.org/10.1016/S0749-6419(03)00100-1.

[13] Y. Choi, et al., Crystal plasticity finite element method simulations for a polycrystalline Ni micro-specimen deformed in tension, Metall. Mater. Trans. 45 (13) (2014) 6352–6359, https://doi.org/10.1007/s11661-014-2556-y.

[14] T.J. Barrett, D.J. Savage, M. Ardeljan, M. Knezevic, An automated procedure for geometry creation and finite element mesh generation: application to explicit grain structure models and machining distortion, Comput. Mater. Sci. 141 (Supplement C) (2018) 269–281, https://doi.org/10.1016/j.commatsci.2017.09.048.

[15] P. Knysh, K. Sasaki, T. Furushima, M. Knezevic, Y.P. Korkolis, A shape interpolation procedure: application to creating explicit grain structure models based on partial data sets, Comput. Mater. Sci. (2019), https://doi.org/10.1016/j.commatsci.2019.05.014.

[16] H. Lim, J.D. Carroll, C.C. Battaile, B.L. Boyce, C.R. Weinberger, Quantitative comparison between experimental measurements and CP-FEM predictions of plastic deformation in a tantalum oligocrystal, Int. J. Mech. Sci. 92 (2015) 98–108.

[17] Y. Guan, B. Chen, J. Zou, T. Ben Britton, J. Jiang, F.P.E. Dunne, Crystal plasticity modelling and HR-DIC measurement of slip activation and strain localization in single and oligo-crystal Ni alloys under fatigue, Int. J. Plast. (2017), https://doi.org/10.1016/j.ijplas.2016.10.001.

[18] Z.W. Hsiao, T.Y. Wu, D. Chen, J.C. Kuo, D.Y. Lin, EBSD and electron channeling study of anomalous slip in oligocrystals of high chromium ferritic stainless steel, Micron (2017), https://doi.org/10.1016/j.micron.2016.12.003.

[19] P. Baudoin, T. Hama, H. Takuda, Influence of critical resolved shear stress ratios on the response of a commercially pure titanium oligocrystal: crystal plasticity simulations and experiment, Int. J. Plast. (2019), https://doi.org/10.1016/j.ijplas.2018.11.013.

[20] M. Schreiber, K.D. Molodov, T. Al-Samman, S. Korte-Kerzel, D.A. Molodov, Impact of grain boundaries on microstructure evolution during deformation of a magnesium tricrystal, Mater. Sci. Eng., A (2019), https://doi.org/10.1016/j.msea.2018.11.002.

[21] S.R. Agnew, O. Duygulu, Plastic anisotropy and the role of non-basal slip in magnesium alloy AZ31B, Int. J. Plast. 21 (6) (2005) 1161–1193, https://doi.org/10.1016/j.ijplas.2004.05.018.

[22] Z. Keshavarz, M.R. Barnett, EBSD analysis of deformation modes in Mg-3Al-1Zn, Scripta Mater. 55 (10) (2006) 915–918 [Online]. Available: http://www.sciencedirect.com/science/article/B6TY2-4KPNHS4-5/2/2b861e221841a9fba6c0f6984eb5e4c4.

[23] S.R. Agnew, C.N. Tomé, D.W. Brown, T.M. Holden, S.C. Vogel, Study of slip mechanisms in a magnesium alloy by neutron diffraction and modeling, Scripta Mater. 48 (8) (2003) 1003–1008, https://doi.org/10.1016/S1359-6462(02)00591-2.

[24] M. Jahedi, B.A. McWilliams, F.R. Kellogg, I.J. Beyerlein, M. Knezevic, Rate and temperature dependent deformation behavior of as-cast WE43 magnesium-rare earth alloy manufactured by direct-chill casting, Mater. Sci. Eng., A 712 (2018) 50–64, https://doi.org/10.1016/j.msea.2017.11.092.

[25] M. Jahedi, B.A. McWilliams, P. Moy, M. Knezevic, Deformation twinning in rolled WE43-T5 rare earth magnesium alloy: influence on strain hardening and texture evolution, Acta Mater. 131 (2017) 221–232, https://doi.org/10.1016/j.actamat.2017.03.075.

[26] E. Vasilev, N.C. Ferreri, R. Decker, I.J. Beyerlein, M. Knezevic, Strain-rate sensitivity, tension-compression asymmetry, r-ratio, twinning, and texture evolution of a rolled magnesium alloy Mg-1.3Zn-0.4Ca-0.4Mn, Metall. Mater. Trans. 51 (8) (2020) 3858–3868, https://doi.org/10.1007/s11661-020-05841-x.

[27] A. Vinogradov, E. Vasilev, M. Linderov, D. Merson, "In situ observations of the kinetics of twinning–detwinning and dislocation slip in magnesium, Mater. Sci. Eng., A 676 (2016) 351–360.

[28] S.R. Agnew, D.W. Brown, C.N. Tomé, Validating a polycrystal model for the elastoplastic response of magnesium alloy AZ31 using in situ neutron diffraction, Acta Mater. 54 (18) (2006) 4841–4852 [Online]. Available: http://www.sciencedirect.com/science/article/B6TW8-4KXDWSD-4/2/b3bcff90751eccc2a4d29d120fe9aabe.

[29] M. Zecevic, I.J. Beyerlein, M. Knezevic, Activity of pyramidal I and II <c+a> slip in Mg alloys as revealed by texture development, J. Mech. Phys. Solid. 111 (2018) 290–307, https://doi.org/10.1016/j.jmps.2017.11.004.

[30] J.W. Christian, S. Mahajan, Deformation twinning, Prog. Mater. Sci. 39 (1–2) (1995) 1–157 [Online]. Available: http://www.sciencedirect.com/science/article/B6TX1-3YRSGDH-1/2/9c86a05bd8433ef810e649a7cfd53862.

[31] S.R. Agnew, M.H. Yoo, C.N. Tome, Application of texture simulation to understanding mechanical behavior of Mg and solid solution alloys containing Li or Y, Acta Mater. 49 (20) (2001) 4277–4289.

[32] S. Ghorbanpour, B.A. McWilliams, M. Knezevic, Low-cycle fatigue behavior of rolled WE43-T5 magnesium alloy, Fatig. Fract. Eng. Mater. Struct. 42 (6) (2019) 1357–1372, https://doi.org/10.1111/ffe.12992.
[33] S. Ghorbanpour, B.A. McWilliams, M. Knezevic, Effect of hot working and aging heat treatments on monotonic, cyclic, and fatigue behavior of WE43 magnesium alloy, Mater. Sci. Eng., A 747 (2019) 27–41, https://doi.org/10.1016/j.msea.2019.01.056.
[34] M. Jahedi, B.A. McWilliams, M. Knezevic, Deformation and fracture mechanisms in WE43 magnesium-rare earth alloy fabricated by direct-chill casting and rolling, Mater. Sci. Eng., A 726 (2018) 194–207, https://doi.org/10.1016/j.msea.2018.04.090.
[35] D.J. Savage, I.J. Beyerlein, N.A. Mara, S.C. Vogel, R.J. McCabe, M. Knezevic, Microstructure and texture evolution in Mg/Nb layered materials made by accumulative roll bonding, Int. J. Plast. 125 (2020) 1–26, https://doi.org/10.1016/j.ijplas.2019.08.015.
[36] S. Ghorbanpour, B.A. McWilliams, M. Knezevic, Effects of environmental temperature and sample pre-straining on high cycle fatigue strength of WE43-T5 magnesium alloy, Int. J. Fatig. 141 (2020), 105903, https://doi.org/10.1016/j.ijfatigue.2020.105903.
[37] M.R. Barnett, Z. Keshavarz, A.G. Beer, D. Atwell, Influence of grain size on the compressive deformation of wrought Mg-3Al-1Zn, Acta Mater. (2004), https://doi.org/10.1016/j.actamat.2004.07.015.
[38] E. Vasilev, D. Merson, A. Vinogradov, Kinetics of twinning and dislocation slip during cyclic deformation of ZK30 magnesium alloy, KnE Eng. 3 (4) (May 2018) 156, https://doi.org/10.18502/keg.v3i4.2238.
[39] M.R. Barnett, A Taylor model based description of the proof stress of magnesium AZ31 during hot working, Metall. Mater. Trans. 34 (9) (2003) 1799–1806.
[40] S.R. Agnew, Plastic Anisotropy of Magnesium Alloy AZ31B Sheet, 2002, https://doi.org/10.1007/978-3-319-48099-2_56.
[41] W.G. Feather, et al., Mechanical response, twinning, and texture evolution of WE43 magnesium-rare earth alloy as a function of strain rate: experiments and multi-level crystal plasticity modeling, Int. J. Plast. 120 (2019) 180–204, https://doi.org/10.1016/j.ijplas.2019.04.019.
[42] W.G. Feather, D.J. Savage, M. Knezevic, A crystal plasticity finite element model embedding strain-rate sensitivities inherent to deformation mechanisms: application to alloy AZ31, Int. J. Plast. 143 (2021), 103031, https://doi.org/10.1016/j.ijplas.2021.103031.
[43] A. Ghaderi, M.R. Barnett, Sensitivity of deformation twinning to grain size in titanium and magnesium, Acta Mater. 59 (20) (2011) 7824–7839, https://doi.org/10.1016/j.actamat.2011.09.018.
[44] B.S. Fromm, B.L. Adams, S. Ahmadi, M. Knezevic, Grain size and orientation distributions: application to yielding of a-titanium, Acta Mater. 57 (8) (2009) 2339–2348 [Online]. Available: http://www.sciencedirect.com/science/article/pii/S1359645409000068.
[45] M. Lentz, et al., "Effect of age hardening on the deformation behavior of an Mg–Y–Nd alloy: in-situ X-ray diffraction and crystal plasticity modeling, Mater. Sci. Eng., A 628 (2015) 396–409, https://doi.org/10.1016/j.msea.2015.01.069.
[46] M. Knezevic, et al., Modeling bending of α-titanium with embedded polycrystal plasticity in implicit finite elements, Mater. Sci. Eng., A 564 (2013) 116–126, https://doi.org/10.1016/j.msea.2012.11.037.
[47] M. Risse, M. Lentz, C. Fahrenson, W. Reimers, M. Knezevic, I.J. Beyerlein, Elevated temperature effects on the plastic anisotropy of an extruded Mg-4 Wt pct Li alloy: experiments and polycrystal modeling, Metall. Mater. Trans. 48 (1) (2017) 446–458.
[48] M. Knezevic, M. Zecevic, I.J. Beyerlein, J.F. Bingert, R.J. McCabe, Strain rate and temperature effects on the selection of primary and secondary slip and twinning systems in HCP Zr, Acta Mater. 88 (2015) 55–73, https://doi.org/10.1016/j.actamat.2015.01.037.
[49] E. Vasilev, M. Zecevic, R.J. McCabe, M. Knezevic, Experimental verification of a crystal plasticity-based simulation framework for predicting microstructure and geometric shape changes: application to bending and Taylor impact testing of Zr, Int. J. Impact Eng. 144 (2020) 103655, https://doi.org/10.1016/j.ijimpeng.2020.103655.
[50] M. Zecevic, I.J. Beyerlein, M. Knezevic, Coupling elasto-plastic self-consistent crystal plasticity and implicit finite elements: applications to compression, cyclic tension-compression, and bending to large strains, Int. J. Plast. 93 (2017) 187–211, https://doi.org/10.1016/j.ijplas.2016.07.016.
[51] A. Chapuis, J.H. Driver, Temperature dependency of slip and twinning in plane strain compressed magnesium single crystals, Acta Mater. 59 (5) (2011) 1986–1994, https://doi.org/10.1016/j.actamat.2010.11.064.
[52] M.A. Meyers, O. Vöhringer, V.A. Lubarda, The onset of twinning in metals: a constitutive description, Acta Mater. 49 (19) (2001) 4025–4039.
[53] M.R. Barnett, M.D. Nave, C.J. Bettles, Deformation microstructures and textures of some cold rolled Mg alloys, Mater. Sci. Eng., A 386 (1–2) (2004) 205–211.
[54] H. Yoshinaga, T. Obara, S. Morozumi, Twinning deformation in magnesium compressed along the C-axis, Mater. Sci. Eng., A 12 (5–6) (1973) 255–264 [Online]. Available: http://www.sciencedirect.com/science/article/B759M-48N5JKT-103/2/e97adc12aac3ca803c488881904dfd5d.
[55] M. Ardeljan, M. Knezevic, Explicit modeling of double twinning in AZ31 using crystal plasticity finite elements for predicting the mechanical fields for twin variant selection and fracture analyses, Acta Mater. 157 (2018) 339–354, https://doi.org/10.1016/j.actamat.2018.07.045.
[56] B.C. Wonsiewicz, W.A. Backofen, Plasticity of magnesium crystals, Trans. Met. Soc. AIME 239 (1967) 1422–1431.
[57] M.R. Barnett, "Twinning and the ductility of magnesium alloys: Part II. 'Contraction' twins, Mater. Sci. Eng., A 464 (1–2) (2007) 8–16 [Online]. Available: http://www.sciencedirect.com/science/article/B6TXD-4N5TN8C-4/2/3ea750c9e55aef479f8f62380676defc.
[58] L. Capolungo, I.J. Beyerlein, Nucleation and stability of twins in hcp metals, Phys. Rev. B 78 (2) (2008), 24117.
[59] L. Capolungo, P.E. Marshall, R.J. McCabe, I.J. Beyerlein, C.N. Tomé, Nucleation and growth of twins in Zr: a statistical study, Acta Mater. 57 (20) (2009) 6047–6056.
[60] R.J. McCabe, G. Proust, E.K. Cerreta, A. Misra, Quantitative analysis of deformation twinning in zirconium, Int. J. Plast. 25 (3) (2009) 454–472, https://doi.org/10.1016/j.ijplas.2008.03.010.
[61] I. Chelladurai, et al., Modeling of trans-grain twin transmission in AZ31 via a neighborhood-based viscoplastic self-consistent model, Int. J. Plast. 117 (2019) 21–32, https://doi.org/10.1016/j.ijplas.2018.03.012.
[62] M.A. Kumar, I.J. Beyerlein, C.N. Tomé, Effect of local stress fields on twin characteristics in HCP metals, Acta Mater. 116 (2016) 143–154.
[63] C. Liu, et al., An integrated crystal plasticity-phase field model for spatially resolved twin nucleation, propagation, and growth in hexagonal materials, Int. J. Plast. (2018), https://doi.org/10.1016/j.ijplas.2018.03.009.
[64] M. Ardeljan, I.J. Beyerlein, M. Knezevic, Effect of dislocation density-twin interactions on twin growth in AZ31 as revealed by explicit crystal plasticity finite element modeling, Int. J. Plast. 99 (Supplement C) (2017) 81–101, https://doi.org/10.1016/j.ijplas.2017.09.002.
[65] M.R. Barnett, Twinning and its role in wrought magnesium alloys, in: C. Bettles, M. Barnett (Eds.), Advances In Wrought Magnesium Alloys: Fundamentals Of Processing, Properties And Applications, 2012, pp. 105–143.
[66] M. Knezevic, A. Levinson, R. Harris, R.K. Mishra, R.D. Doherty, S.R. Kalidindi, Deformation twinning in AZ31: influence on strain hardening and texture evolution, Acta Mater. 58 (19) (2010) 6230–6242 [Online]. Available: http://www.sciencedirect.com/science/article/pii/S1359645410004854.
[67] M.R. Barnett, Importance of propagation in controlling the twinning stress in Mg, Scripta Mater. 162 (2019) 447–450.
[68] E.W. Kelley, J.W.F. Hosford, Plane strain compression of magnesium and magnesium alloy crystals, Metall. Soc. Am. Inst. Mining, Metall. Pet. Eng. – Trans. 224 (1968) 5–13.
[69] M. Ardeljan, I.J. Beyerlein, B.A. McWilliams, M. Knezevic, Strain rate and temperature sensitive multi-level crystal plasticity model for large plastic deformation behavior: application to AZ31 magnesium alloy, Int. J. Plast. 83 (2016) 90–109, https://doi.org/10.1016/j.ijplas.2016.04.005.
[70] M. Knezevic, et al., Modeling mechanical response and texture evolution of α-uranium as a function of strain rate and temperature using polycrystal plasticity, Int. J. Plast. 43 (2013) 70–84, https://doi.org/10.1016/j.ijplas.2012.10.011.
[71] W.B. Hutchinson, M.R. Barnett, Effective values of critical resolved shear stress for slip in polycrystalline magnesium and other hcp metals, Scripta Mater. (2010), https://doi.org/10.1016/j.scriptamat.2010.05.047.
[72] I.J. Beyerlein, R.J. McCabe, C.N. Tomé, Effect of microstructure on the nucleation of deformation twins in polycrystalline high-purity magnesium: a multi-scale modeling study, J. Mech. Phys. Solid. 59 (5) (2011) 988–1003 [Online]. Available: http://www.sciencedirect.com/science/article/pii/S0022509611000354.
[73] M.R. Barnett, A. Ghaderi, J.Q. Da Fonseca, J.D. Robson, Influence of orientation on twin nucleation and growth at low strains in a magnesium alloy, Acta Mater. 80 (2014) 380–391.
[74] Y. Pei, A. Godfrey, J. Jiang, Y.B. Zhang, W. Liu, Q. Liu, Extension twin variant selection during uniaxial compression of a magnesium alloy, Mater. Sci. Eng., A 550 (2012) 138–145.
[75] T.R. Bieler, R. Alizadeh, M. Peña-Ortega, J. Llorca, An analysis of (the lack of) slip transfer between near-cube oriented grains in pure Al, Int. J. Plast. 118 (2019) 269–290, https://doi.org/10.1016/j.ijplas.2019.02.014.
[76] I.J. Beyerlein, C.N. Tomé, A probabilistic twin nucleation model for HCP polycrystalline metals, Proc. R. Soc. A Math. Phys. Eng. Sci. 466 (2121) (2010) 2517–2544, https://doi.org/10.1098/rspa.2009.0661.
[77] M.R. Barnett, Z. Keshavarz, A.G. Beer, X. Ma, Non-Schmid behaviour during secondary twinning in a polycrystalline magnesium alloy, Acta Mater. 56 (1) (2008) 5–15 [Online]. Available: http://www.sciencedirect.com/science/article/B6TW8-4R2GS3J-1/2/e16d5b3e2e642e55dc7015e77f1b323e.
[78] M. Knezevic, et al., Integration of self-consistent polycrystal plasticity with dislocation density based hardening laws within an implicit finite element framework: application to low-symmetry metals, J. Mech. Phys. Solid. 61 (10) (2013) 2034–2046, https://doi.org/10.1016/j.jmps.2013.05.005.
[79] R.E. Reed-Hill, W.D. Robertson, Additional modes of deformation twinning in magnesium, Acta Metall. 5 (12) (1957) 717–727.
[80] D. Ando, J. Koike, Y. Sutou, The role of deformation twinning in the fracture behavior and mechanism of basal textured magnesium alloys, Mater. Sci. Eng., A (2014), https://doi.org/10.1016/j.msea.2014.02.010.
[81] J. Koike, N. Fujiyama, D. Ando, Y. Sutou, Roles of deformation twinning and dislocation slip in the fatigue failure mechanism of AZ31 Mg alloys, Scripta Mater. (2010), https://doi.org/10.1016/j.scriptamat.2010.03.021.
[82] P. Cizek, M.R. Barnett, Characteristics of the contraction twins formed close to the fracture surface in Mg-3Al-1Zn alloy deformed in tension, Scripta Mater. 59 (9) (2008) 959–962 [Online]. Available: http://www.sciencedirect.com/science/article/B6TY2-4SX3P4G-1/2/5d9e255fc04ff06f7f2cf3de2b372fe5.
[83] M. Lentz, M. Klaus, I.J. Beyerlein, M. Zecevic, W. Reimers, M. Knezevic, "In situ X-ray diffraction and crystal plasticity modeling of the deformation behavior of extruded Mg–Li–(Al) alloys: an uncommon tension–compression asymmetry, Acta Mater. 86 (2015) 254–268, https://doi.org/10.1016/j.actamat.2014.12.003.

[84] I.J. Beyerlein, J. Wang, M.R. Barnett, C.N. Tomé, Double twinning mechanisms in magnesium alloys via dissociation of lattice dislocations, Proc. R. Soc. A Math. Phys. Eng. Sci. 468 (2141) (2012) 1496–1520.
[85] T.R. Bieler, L. Wang, A.J. Beaudoin, P. Kenesei, U. Lienert, In situ characterization of twin nucleation in pure Ti using 3D-XRD, Metall. Mater. Trans. 45 (1) (2014) 109–122.
[86] B.M. Morrow, R.J. McCabe, E.K. Cerreta, C.N. Tomé, In-situ TEM observation of twinning and detwinning during cyclic loading in Mg, Metall. Mater. Trans. 45 (1) (2014) 36–40, https://doi.org/10.1007/s11661-013-1765-0.
[87] M. Zecevic, M. Knezevic, I.J. Beyerlein, C.N. Tomé, An elasto-plastic self-consistent model with hardening based on dislocation density, twinning and de-twinning: application to strain path changes in HCP metals, Mater. Sci. Eng., A 638 (2015) 262–274, https://doi.org/10.1016/j.msea.2015.04.066.
[88] M. Knezevic, I.J. Beyerlein, D.W. Brown, T.A. Sisneros, C.N. Tomé, A polycrystal plasticity model for predicting mechanical response and texture evolution during strain-path changes: application to beryllium, Int. J. Plast. 49 (2013) 185–198, https://doi.org/10.1016/j.ijplas.2013.03.008.
[89] C.M. Cepeda-Jiménez, J.M. Molina-Aldareguia, M.T. Pérez-Prado, Effect of grain size on slip activity in pure magnesium polycrystals, Acta Mater. (2015), https://doi.org/10.1016/j.actamat.2014.10.001.
[90] C.J. Boehlert, Z. Chen, I. Gutiérrez-Urrutia, J. Llorca, M.T. Pérez-Prado, In situ analysis of the tensile and tensile-creep deformation mechanisms in rolled AZ31, Acta Mater. (2012), https://doi.org/10.1016/j.actamat.2011.10.025.
[91] Z.R. Zeng, M.Z. Bian, S.W. Xu, C.H.J. Davies, N. Birbilis, J.F. Nie, Effects of dilute additions of Zn and Ca on ductility of magnesium alloy sheet, Mater. Sci. Eng., A (2016), https://doi.org/10.1016/j.msea.2016.07.049.
[92] T.R. Bieler, et al., The role of heterogeneous deformation on damage nucleation at grain boundaries in single phase metals, Int. J. Plast. 25 (9) (2009) 1655–1683, https://doi.org/10.1016/j.ijplas.2008.09.002.
[93] P.J. Withers, H.K.D.H. Bhadeshia, Residual stress part 1 - measurement techniques, Mater. Sci. Technol. (2001), https://doi.org/10.1179/026708301101509980.
[94] M. Zecevic, Y.P. Korkolis, T. Kuwabara, M. Knezevic, "Dual-phase steel sheets under cyclic tension–compression to large strains: experiments and crystal plasticity modeling, J. Mech. Phys. Solid. 96 (2016) 65–87, https://doi.org/10.1016/j.jmps.2016.07.003.
[95] M. Zecevic, M. Knezevic, Latent hardening within the elasto-plastic self-consistent polycrystal homogenization to enable the prediction of anisotropy of AA6022-T4 sheets, Int. J. Plast. 105 (2018) 141–163, https://doi.org/10.1016/j.ijplas.2018.02.007.
[96] Z. Feng, et al., A comparative study between elasto-plastic self-consistent crystal plasticity and anisotropic yield function with distortional hardening formulations for sheet metal forming, Mech. Mater. 148 (2020), 103422, https://doi.org/10.1016/j.mechmat.2020.103422.
[97] T.J. Barrett, M. Knezevic, "Deep drawing simulations using the finite element method embedding a multi-level crystal plasticity constitutive law: experimental verification and sensitivity analysis,", Comput. Methods Appl. Mech. Eng. 354 (2019) 245–270, https://doi.org/10.1016/j.cma.2019.05.035.
[98] M. Zecevic, M. Knezevic, A dislocation density based elasto-plastic self-consistent model for the prediction of cyclic deformation: application to Al6022-T4, Int. J. Plast. 72 (2015) 200–217.
[99] M. Zecevic, M. Knezevic, An implicit formulation of the elasto-plastic self-consistent polycrystal plasticity model and its implementation in implicit finite elements, Mech. Mater. 136 (2019), 103065, https://doi.org/10.1016/j.mechmat.2019.103065.
[100] S. Ghorbanpour, et al., A crystal plasticity model incorporating the effects of precipitates in superalloys: application to tensile, compressive, and cyclic deformation of Inconel 718, Int. J. Plast. 99 (Supplement C) (2017) 162–185, https://doi.org/10.1016/j.ijplas.2017.09.006.
[101] J. Wang, M. Zecevic, M. Knezevic, I.J. Beyerlein, Polycrystal plasticity modeling for load reversals in commercially pure titanium, Int. J. Plast. 125 (2020) 294–313, https://doi.org/10.1016/j.ijplas.2019.09.013.
[102] A.M. Kumar, A.K. Kanjarla, S.R. Niezgoda, R.A. Lebensohn, C.N. Tomé, Numerical study of the stress state of a deformation twin in magnesium, Acta Mater. 84 (2015) 349–358, https://doi.org/10.1016/j.actamat.2014.10.048.
[103] M. Ardeljan, R.J. McCabe, I.J. Beyerlein, M. Knezevic, Explicit incorporation of deformation twins into crystal plasticity finite element models, Comput. Methods Appl. Mech. Eng. 295 (2015) 396–413, https://doi.org/10.1016/j.cma.2015.07.003.
[104] A.S. Khan, A. Pandey, T. Gnaupel-Herold, R.K. Mishra, Mechanical response and texture evolution of AZ31 alloy at large strains for different strain rates and temperatures, Int. J. Plast. 27 (5) (2011) 688–706, https://doi.org/10.1016/j.ijplas.2010.08.009.
[105] J.J. Jonas, S. Mu, T. Al-Samman, G. Gottstein, L. Jiang, Ė. Martin, The role of strain accommodation during the variant selection of primary twins in magnesium, Acta Mater. 59 (5) (2011) 2046–2056.
[106] H. Abdolvand, M. Majkut, J. Oddershede, J.P. Wright, M.R. Daymond, "Study of 3-D stress development in parent and twin pairs of a hexagonal close-packed polycrystal: Part I – in-situ three-dimensional synchrotron X-ray diffraction measurement, Acta Mater. 93 (2015) 246–255, https://doi.org/10.1016/j.actamat.2015.04.020.
[107] M. Knezevic, M.R. Daymond, I.J. Beyerlein, Modeling discrete twin lamellae in a microstructural framework, Scripta Mater. 121 (2016) 84–88, https://doi.org/10.1016/j.scriptamat.2016.04.026.
[108] K.D. Molodov, T. Al-Samman, D.A. Molodov, Profuse slip transmission across twin boundaries in magnesium, Acta Mater. (2017), https://doi.org/10.1016/j.actamat.2016.11.022.
[109] B.B. Rath, I.M. Bernstein, The relation between grain-boundary orientation and intergranular cracking, Metall. Trans. (1971), https://doi.org/10.1007/BF02813262.
[110] S.P. Lynch, P. Trevena, Stress corrosion cracking and liquid metal embrittlement IN pure magnesium, Corrosion (1988), https://doi.org/10.5006/1.3583907.
[111] A. Serra, D.J. Bacon, Computer simulation of screw dislocation interactions with twin boundaries in H.C.P. metals, Acta Metall. Mater. (1995), https://doi.org/10.1016/0956-7151(95)00128-I.
[112] D. Meyn, E. Brooks, Microstructural origin of flutes and their use in distinguishing striationless fatigue cleavage from stress-corrosion cracking in titanium alloys, in: " Fractography and Materials Science, 2009.
[113] B. Cox, Environmentally-induced cracking of zirconium alloys - a review, J. Nucl. Mater. (1990), https://doi.org/10.1016/0022-3115(90)90321-D.
[114] T. Motooka, K. Kiuchi, Corrosion fatigue growth of zirconium in boiling nitric acid, Corrosion (2002), https://doi.org/10.5006/1.3277645.
[115] D.B. Prabhu, S. Dhamotharan, G. Sathishkumar, P. Gopalakrishnan, K.R. Ravi, "Stress corrosion cracking of biodegradable Mg-4Zn alloy in simulated body fluid at different strain rates – a fractographic investigation, Mater. Sci. Eng., A (2018), https://doi.org/10.1016/j.msea.2018.06.002.